

# SMC Bulletin

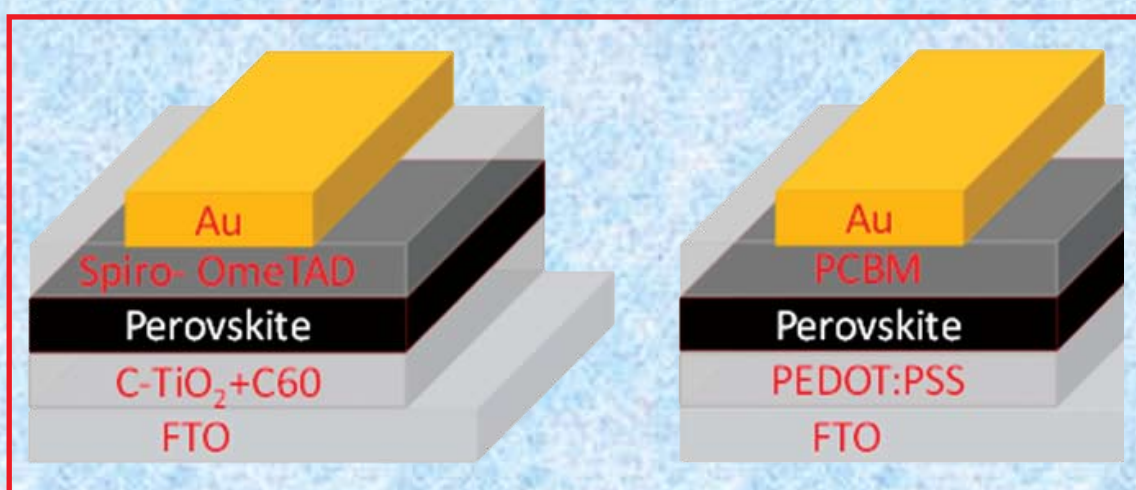
ISSN 2394-5087

A Publication of the Society for Materials Chemistry

Volume 8

Nos. 2

August 2017



**Special Issue on Electronic Materials**



# Society for Materials Chemistry

Society for Materials Chemistry was mooted in 2007 with following aims and objectives:

- (a) to help the advancement, dissemination and application of the knowledge in the field of materials chemistry,
- (b) to promote active interaction among all material scientists, bodies, institutions and industries interested in achieving the advancement, dissemination and application of the knowledge of materials chemistry,
- (c) to disseminate information in the field of materials chemistry by publication of bulletins, reports, newsletters, journals.
- (d) to provide a common platform to young researchers and active scientists by arranging seminars, lectures, workshops, conferences on current research topics in the area of materials chemistry,
- (e) to provide financial and other assistance to needy deserving researchers for participation to present their work in symposia, conference, etc.
- (f) to provide an incentive by way of cash awards to researchers for best thesis, best paper published in journal/national/international conferences for the advancement of materials chemistry,
- (g) to undertake and execute all other acts as mentioned in the constitution of SMC.

## Executive Committee

### President

**Dr. V. K. Jain**

Bhabha Atomic Research Centre  
Trombay, Mumbai, 400 085  
[jainvk@barc.gov.in](mailto:jainvk@barc.gov.in)

### Vice-Presidents

**Dr. A. K. Tyagi**

Bhabha Atomic Research Centre  
Trombay, Mumbai, 400 085  
[jainvk@barc.gov.in](mailto:jainvk@barc.gov.in)

**Dr. C. S. Sundar**

J.C. Bose Fellow & Sr. Professor,  
HBNI Materials Science Group  
Indira Gandhi Centre for Atomic  
Research Kalpakkam, 603102  
[css@igcar.gov.in](mailto:css@igcar.gov.in)

### Secretary

**Dr. P. A. Hassan**

Bhabha Atomic Research Centre  
Trombay, Mumbai, 400 085  
[hassan@barc.gov.in](mailto:hassan@barc.gov.in)

### Treasurer

**Dr. Sandeep Nigam**

Bhabha Atomic Research Centre  
Trombay, Mumbai, 400 085  
[snigam@barc.gov.in](mailto:snigam@barc.gov.in)

### Members

**Dr. K. C. Barick**  
Bhabha Atomic Research Centre  
Trombay, Mumbai-400085

**Dr. S. Kannan**

Bhabha Atomic Research Centre  
Trombay, Mumbai-400085

**Shri. R. K. Mishra**

Bhabha Atomic Research Centre  
Trombay, Mumbai-400085

**Dr. Ratikant Mishra**

Bhabha Atomic Research Centre  
Trombay, Mumbai-400085

**Dr. G. Mugesh**

Indian Institute of Science  
Bangalore-560012

**Dr. (Smt.) Mrinal Pai**

Bhabha Atomic Research Centre  
Trombay, Mumbai-400085

**Dr. Vivek Polshettiwar**

Tata Institute Atomic Research Centre  
Colaba, Mumbai-400005

**Dr. S. K. Sarkar**

Raja Ramanna Fellow  
Bhabha Atomic Research Centre  
Trombay, Mumbai-400085

**Dr. A. K. Tripathi**

Bhabha Atomic Research Centre  
Trombay, Mumbai-400085

**Dr. R. K. Vatsa**

Bhabha Atomic Research Centre  
Trombay, Mumbai-400085

**Dr. V. Venugopal**

Raja Ramanna Fellow  
Bhabha Atomic Research Centre  
Trombay, Mumbai-400085

### Co-opted Members

**Prof. Anshu Dandia**

University of Rajasthan  
Jaipur-302004

**Dr. D. Das**

Raja Ramanna Fellow  
Bhabha Atomic Research Centre  
Trombay, Mumbai-400085

**Prof. A. K. Ganguli**

Institute of Nano Science  
and Technology  
Mohali, Punjab - 160062

**Dr. K. M. Parida**

Institute of Technical Education  
& Research  
Siksha 'O' Anusandhan University  
Bhubaneswar-751030

**Dr. V. Sudarsan**

Bhabha Atomic Research Centre  
Trombay, Mumbai-400085

---

Contact address

**Society for Materials Chemistry**

C/o Chemistry Division

Bhabha Atomic Research Centre, Trombay, Mumbai, 400 085, India

Tel: +91-22-25592001, E-mail: [socmatchem@gmail.com](mailto:socmatchem@gmail.com)

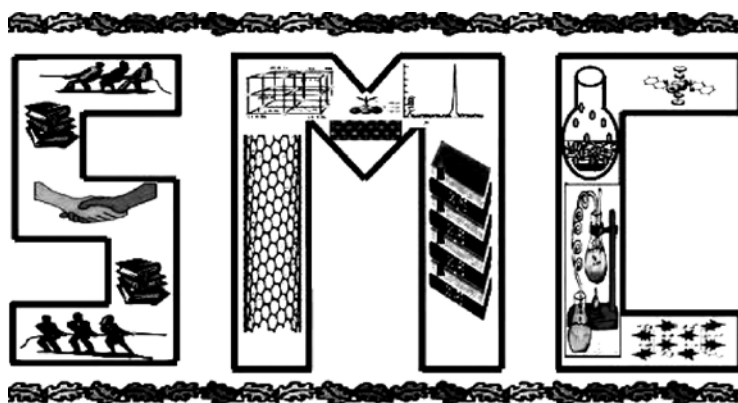
# SMC Bulletin

A Publication of the Society for Materials Chemistry

Volume 8

No. 2

August 2017



SOCIETY FOR MATERIALS CHEMISTRY

# SMC Bulletin

Vol. 8

Nos. 2

August 2017

## Guest Editor

### Prof. K. L. Narasimhan

Distinguished Visiting Professor  
Department of Electrical Engineering  
Indian Institute of Technology Bombay,  
Powai Mumbai-400 076

Editorial Board	
<b>Dr. Arvind Kumar Tripathi</b> Chemistry Division Bhabha Atomic Research Centre Trombay, Mumbai, 400 085 e-mail: catal@barc.gov.in	
<b>Dr. Manidipa Basu</b> Chemistry Division Bhabha Atomic Research Centre Trombay, Mumbai, 400 085 e-mail: deepa@barc.gov.in	<b>Dr. Rajesh Ganesan</b> Materials Chemistry Division Indira Gandhi Centre for Atomic Research, Kalpakkam, 603102 e-mail: rajesh@igcar.gov.in
<b>Dr. G. Kedarnath</b> Chemistry Division Bhabha Atomic Research Centre Trombay, Mumbai, 400 085 e-mail: deepa@barc.gov.in	<b>Dr. Sandeep Nigam</b> Chemistry Division Bhabha Atomic Research Centre Trombay, Mumbai, 400 085 e-mail: snigam@barc.gov.in
<b>Dr. Rajesh V. Pai</b> Fuel Chemistry Division Bhabha Atomic Research Centre Trombay, Mumbai, 400 085 e-mail: rajeshvp@barc.gov.in	<b>Dr. Vivek Polshettiwar</b> Department of Chemical Sciences, Tata Institute of Fundamental Research, Colaba, Mumbai 400005 e-mail: vivekpol@tifr.res.in

---

## Published by

Society for Materials Chemistry  
C/o. Chemistry Division  
Bhabha Atomic Research Centre, Trombay, Mumbai, 400 085  
E-mail: socmatchem@gmail.com, Tel: +91-22-25592001

*Please note that the authors of the paper are alone responsible for the technical contents of papers and references cited therein.  
Front cover shows device architectures of normal and inverted perovskite solar cells.*

---

---

## *Guest Editorial*

---

---



**Prof. K. L. Narasimhan**

Materials play a very important role in modern electronics. Given the diversity of materials and processes and synthesis, no journal can hope to capture the richness and complexities of this field. However, timely reviews enable young researchers to be abreast of the developments in the field. It is also hoped that these reviews will attract the attention of researchers to enable cross pollination across disciplines. This special issue on electronic materials attempts to provide readers a small perspective and a flavor of the role of materials processing in electronics and energy. The articles in this issue emphasize synthesis and processing. The article by Dr. P.K. Basu highlights the importance of chemical processing to provide micro textured surfaces on silicon to reduce reflectance and lower contact resistance for industrial solar cells. Perovskite materials have attracted a lot of attention in recent years. Dr. Pabitra Nayak's article addresses materials and chemistry issues on the synthesis of metal halide perovskites for use as thin film solar cells. Nano materials play an important role in microelectronics. The review by Dr. Anshu Pandey and co-workers review the role of nucleation in the control of morphology and size dispersivity of nanocrystals- which is very important for practical applications. One of the important future directions of electronics is flexible wearable electronics. The article by Dr. Deepak Kumar and co-workers summarises some recent developments in both organic and metal oxide electronics. Organic material synthesis is key for the development of flexible electronics. The review by Dr. Anil Kumar and Dr. Sreelekha Sunil describes recent advances in flowchemistry for the synthesis of conjugated semiconductors.

It has been a pleasure and a privilege to be an editor for this special issue on "*Electronic Materials*". I thank the editorial board of SMC for this opportunity. Putting this issue together was only possible because of the contributions of the authors who despite many demands on their time kindly agreed to write up the articles and submit them in a reasonable time frame. I take this opportunity to thank all the authors for their contribution.



---

---

## From the desks of the President and Secretary

---

---



**Dr. V.K. Jain**  
*President*



**Dr. P. A. Hassan**  
*Secretary*

Dear Fellow Members and Readers,

Greeting from the Executive Council of SMC

As you are aware, SMC has been in the forefront of updating our members with the scientific advancements in frontier areas relevant to materials science. This time too, we are back with a special issue on electronic materials. Remarkable progress has been made in the area of semiconductor technology to meet the ever-increasing demands of energy consumption world over. This has led to an enormous growth in harnessing all means of energy sources available. To make India's economic development energy-efficient, the Government of India initiated a National Solar Mission. In view of these developments, it is appropriate to have a special issue on "Electronic Materials".

Development of new materials or processes for solar photovoltaics is of utmost importance considering the high cost of solar power compared to fossil fuels. The importance of surface nano- structuring to improve the efficiency of silicon based solar photovoltaics is brought out in the lead article in this issue. Metal halide perovskites are emerging as a new class of semiconductor materials which is expected to become a core component in many electronic devices. Colloids based processing of such materials to thin film devices remains a challenging task. The role of solvent and colloid chemistry in achieving this objective is being discussed. Fundamental understanding of nucleation and growth of nanocrystals is of utmost relevance for the bottom up processing of semiconductors. We bring to the attention of our readers the science of colloid based processing of materials.

Polymers technology has revolutionised all aspects of human life. Conventional polymers are electrically insulating. Now it has become evident that polymers can be made conducting by introducing conjugated pi bonds and this has made its entry into the field of electronic materials. Recent advances in the area of conjugated polymers and organic thin film transistors for flexible devices and new processing methodologies for organic devices are being discussed in this issue.

We are extremely thankful to the Guest Editor, Prof. K. L. Narasimhan and all the contributing authors for sharing their knowledge and highlighting the recent advances in this area. We are sure that this issue will play a pivotal role in knowledge sharing in the development of advanced electronic materials, with special reference to photovoltaics and display devices. We thank all our readers for their patronage and continued support in the growth of the Society.





# CONTENTS

Features Articles	Page No.
1. <b>Alkaline pyramidal texturing processes for industrial monocrystalline silicon wafer solar cells</b> <i>Prabir Kanti Basu</i>	1
2. <b>Role of colloids and solvent chemistry in metal halide perovskites thin film and crystal formation.</b> <i>Pabitra K. Nayak</i>	7
3. <b>Controlling Nucleation and Growth to Engineer Nanocrystal Composition and Morphology</b> <i>Rekha Mahadevu, Dev Kumar Thapa, Biswajit Bhattacharyya and Anshu Pandey</i>	13
4. <b>Advances in Flexible Thin-Film Transistors and Their Applications</b> <i>Ashutosh Kumar Tripathi, Ishan Choudhary, Deepak</i>	21
5. <b>Conjugated Polymers: New Insights via Continuous Flow Syntheses</b> <i>Anil Kumar and Sreelekha P Gopinathan</i>	28



# Alkaline pyramidal texturing processes for industrial monocrystalline silicon wafer solar cells

Prabir Kanti Basu

National Centre for Photovoltaic Research and Education (NCPRE), Indian Institute of Technology Bombay  
Electrical Engineering Department, Powai, Mumbai - 400076, Maharashtra, India

E-mail: prabir\_basu64@rediffmail.com

## Abstract

Reduction in optical losses in monocrystalline silicon (c-Si) solar cells by surface texturing is one of the important issues of modern silicon photovoltaics (PV). Formation of random pyramidal structure by anisotropic selective etching of <100> oriented c-Si wafers is the de-facto process. The textured surface reduces optical reflectance due to the so-called 'double-bounce' effect. Smaller (heights ~2-4  $\mu\text{m}$ ), but uniform pyramids are essential for better solar cell electrical parameters. Low concentration sodium hydroxide (NaOH) or potassium hydroxide (KOH) based solutions are commonly used as a low-cost, reproducible and high throughput industrial texturing process. Researchers have also applied tetra-methyl ammonium hydroxide, tribasic sodium phosphate, hydrazine mono-hydrate, etc., based solutions in place of NaOH or KOH. Isopropyl alcohol (IPA) is generally mixed in the texture solution to modify the Si-surface wettability for controlled nucleation of pyramids. However, cost of IPA is a serious concern for the industrial texturing process. Replacing IPA by suitable alternatives or reduction of IPA consumption without affecting process quality and process cost are the other areas of research. In this work a review of available industrial alkaline texturing processes is reported in brief. Some of them are regularly used in a PV industry.

## Introduction

Crystalline silicon (Si) is a high refractive index (~3.5) material and thus nearly 30% of light is getting reflected upon incidence onto it. These reflection losses can be directly correlated with loss of photogenerated carriers responsible for photovoltaic (PV) effect. Thus reduction of optical losses in crystalline Si solar cells by surface texturing is one of the important issues of modern silicon PV. For the monocrystalline Si (c-Si) wafers, many researchers [1,2] have shown the selective etching of <100> oriented Si by using sodium hydroxide (NaOH) or potassium hydroxide (KOH) solution. For c-Si solar cells, these anisotropic etches are used to form pyramidal structure that can collect the reflected light and trap the light inside the cells by repeated reflections [3,4]. In order to enhance the pyramid nucleation, the interfacial energy of Si/electrolyte should be reduced, so that sufficient wettability for the Si-surface can be achieved. Isopropyl alcohol (IPA) is generally mixed in the textured solution in order to achieve good uniformity of pyramidal structure on the c-Si surface [5,6].

Uniform pyramidal texturing is also critical from the point of view of making proper front silver (Ag) contact on the emitter surface of the c-Si solar cells. Researchers investigated this influence using boron-doped *p*-type c-Si cells with a controlled variation of the pyramid heights in alkaline texturization process [7,8]. It is observed that cell groups fabricated on wafers with smaller (heights ~2-4  $\mu\text{m}$ )

pyramids achieve higher average fill factor (*FF*) and lower average specific contact resistance than cell groups fabricated on wafers with larger pyramids. Microstructure investigations of the Ag/*n*<sup>+</sup> Si contact interface reveal that most Ag crystallite growth is concentrated around the upper part of the pyramids [8] and hence pyramid density is identified as an important parameter influencing contact formation.

Several researchers have tried to replace KOH/NaOH based solutions with alternative chemical solutions including: tetra-methyl ammonium hydroxide (TMAH) [9], tribasic sodium phosphate ( $\text{Na}_3\text{PO}_4 \cdot 12\text{H}_2\text{O}$ ) [10], hydrazine mono-hydrate ( $\text{N}_2\text{H}_4 \cdot \text{H}_2\text{O}$ ) [11], sodium carbonate/bicarbonate ( $\text{Na}_2\text{CO}_3/\text{NaHCO}_3$ ) [12]. However, in each case IPA is still required for pyramid nucleation. Other group of researchers investigated the use of additives to eliminate the use of IPA in texturing [13-18]. For IPA-free texturing, chemical bench equipment vendors, i.e., RENA GmbH [19], Stangl GmbH [20], and commercial chemical suppliers, i.e., Dow Chemical [21], GP Solar [22], have developed own processes with their additives. Basu *et al.* [23] reported a process using silicate additive to reduce the IPA consumption in texturing.

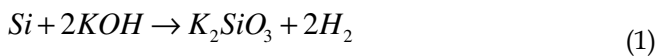
Till 2015 the c-Si wafer sawing technology was dominated by the multi-wire-slurry-sawing (MWSS) technology [24]. Critical issues like environmental, steel-wire breakage rate, low productivity and high kerf-loss [25] are associated with the MWSS process. A new Si wafer

sawing technique, known as diamond-wire-sawing (DWS) [26] overcomes these difficulties with its high throughput, higher yield, longer wire lifetime, convenient cooling liquid recycling and low kerf-loss [27] features. Presently, the DWS c-Si wafers dominate PV market. The MWSS wafers have thick damaged layer (~10 μm) with random distribution of broken crystals and the DWS wafers have shiny surface with a less damaged layer (~5 μm) with ~10-20 nm amorphous silicon (a-Si) layer over and above the damaged layer [26]. Shiny Si-surface with a-Si layer generates difficulties in conventional alkaline texturing. Researchers have overcome these difficulties using different saw damage removal (SDR) processes [26, 28].

In this study a review of the different industrial alkaline texturing processes for pyramidal texturing for c-Si wafers is reported. It includes understanding of the chemical processes and mechanisms related to texturing to generate uniform smaller pyramids with ~2-4 μm height with simultaneous realization of low weighted average reflectance (WAR) of ~2.5% after amorphous silicon nitride (SiN<sub>x</sub>) antireflection coating (ARC) deposition. The texturing processes was generally applied on industrial-grade 6 inch pseudo-square CZ c-Si wafers (boron doped, p-type, <100> orientation, ~2 Ω-cm resistivity, 160-180 μm thickness).

## Results and Discussion

The use of a low concentration of alkalis, i.e., KOH or NaOH solutions for pyramidal texturing of <100> oriented c-Si wafers lies in its anisotropic Si-etching property. The alkali solution has the highest etching rate of the (100) plane and the lowest for the (111) plane [29-31]. Seidel *et al.* [32] attributed this etch-rate variation to the number of dangling bonds for the surface Si atoms for each unit cell. The (100) orientation have two dangling bonds and thus etch faster as compared to (111) plane with only one dangling bond. During the chemical process, before the formation of the silicon hydroxide complex, three Si-Si back bonds need to be broken for (111) plane, however, for (100), two back-bonds to break [32]. Si surface is hydrogen terminated during alkaline etching [31] and alkaline solution is the active species with hydroxyl ions (OH<sup>-</sup>) which catalyze the chemical reaction. The final by-products are potassium silicate (K<sub>2</sub>SiO<sub>3</sub>) and hydrogen (H<sub>2</sub>) gas [15]:



It is also reported that low concentration of alkaline solution generates higher polymerization of silicate complex [31]. On controlled etching of <100> Si planes, <111> planes got exposed to auto-stop Si-etching process

and thus formation of pyramids results [29]. This gives an opportunity for <100> oriented Si wafer to form pyramidal textured surface.

The reflection reduction from the pyramidal surface can be understood from a simple 2D diagram of Figure 1 [31]. On first incidence at point 'a', 70% of this light is absorbed/transmitted into Si-surface. The rest (30%) light is now have

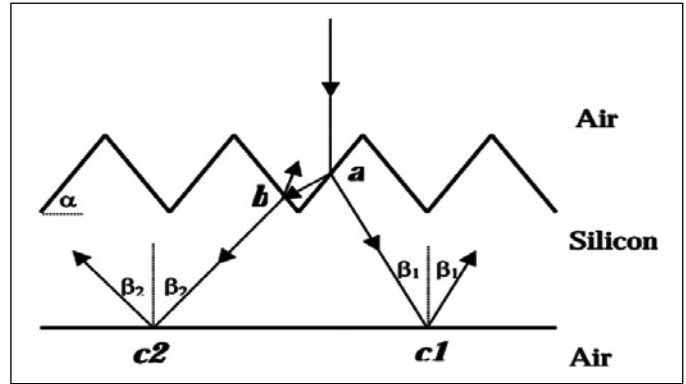


Fig. 1: Reflection reduction process for double bounce pyramidal textured surface [31].

a second incidence on the neighbouring pyramidal face at point 'b' and so additional 70% of the remaining 30%, i.e., 21% of the incident light is getting absorbed/transmitted into Si-surface. This way reflection loss is reduced from 30% to 9% only. There is also a possibility of more than two incidences depending on the facet angles. Generally, 30° and 54° facet angles are necessary for two and three bounce of light respectively [31].

Figure 2 shows the actual images (taken by scanning electron microscope (SEM)) of the pyramids formed during the alkaline KOH-IPA based texturing process. The surface reflectance of a c-Si wafer at different stages of processing is shown in Figure 3. The WAR of the final ARC textured wafer is 2.3% after starting from WAR of 31.8% for the as-cut DWS c-Si wafer. The complete alkaline pyramidal texturization process for c-Si wafers consists of mainly three steps. In the first step, the saw damages on the wafers were removed by alkaline or wafers were removed by alkaline or acidic solutions in the SDR or pre-treatment step [31].

Next, the pyramid formation happens in alkali based texturing solutions (namely 'pyramidal texturing step') followed by neutralization of residual alkali traces in hydrochloric (HCl) acid based solutions. Every chemical processing steps always have a de-ionized water (DIW) rinsing step in between. The complete process flow of any alkaline texturing process is shown in Figure 4. Several approaches are available for the SDR processes, however, in this work, different approaches of pyramidal texturing are only explained.

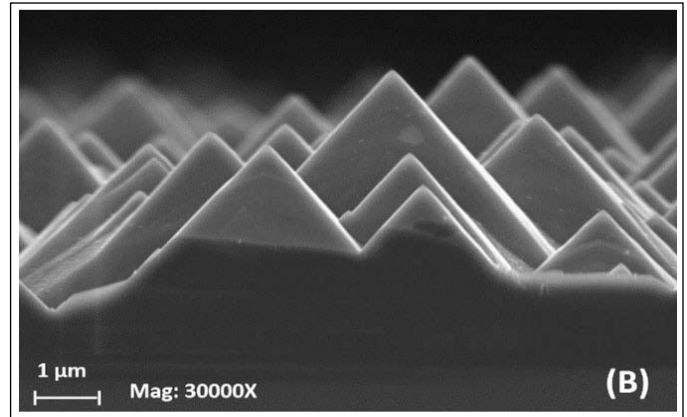
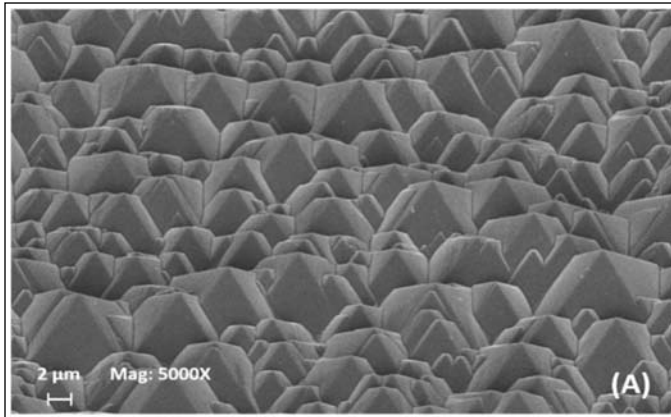


Fig. 2: SEM micrographs of the alkaline textured c-Si wafer surfaces: (A) Angular view 45°, magnification = 5000X, (B) Side view, magnification = 30000X.

The pyramidal texturing process can be classified into three major groups. One group uses KOH (or NaOH) based texturing solution mixed with IPA. The second group replaces KOH (or NaOH) completely. However, they may be using IPA or not. The last group does not use IPA at all during texturing. All the processes for these groups are discussed separately.

### 2.1 Group-1: Pyramidal texturing with KOH/NaOH and IPA

One of the by-product in texturing chemical reaction is the evolution of H<sub>2</sub> bubbles (Eqn.(1)). During texturing, the H<sub>2</sub> bubbles then covers the Si-surface locally by sticking to the wafer surface. These covered areas thus got unexposed towards the texturing solution and pyramid formation stops on those places. So non-uniform texturing results over the entire Si surface. The role of IPA is to enhance Si surface wettability by preventing H<sub>2</sub> bubble to adhere on the Si surface. The effective removal of H<sub>2</sub> bubbles from the entire Si wafer surface maintains a consistent chemical

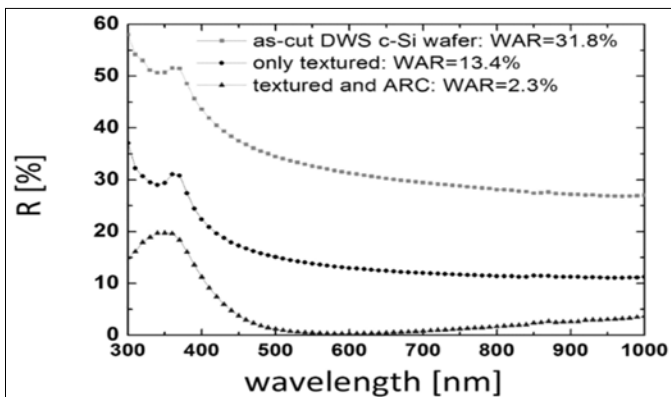


Fig. 3: The variation of surface reflectance (R) and the weighted average reflectance (WAR) of the DWS c-Si wafer at conditions as as-cut before texturing, after texturing and after deposition of ARC SiN<sub>x</sub> layer. WAR value is weighted using the AM1.5G solar spectrum over the 300-1000 nm wavelength range.

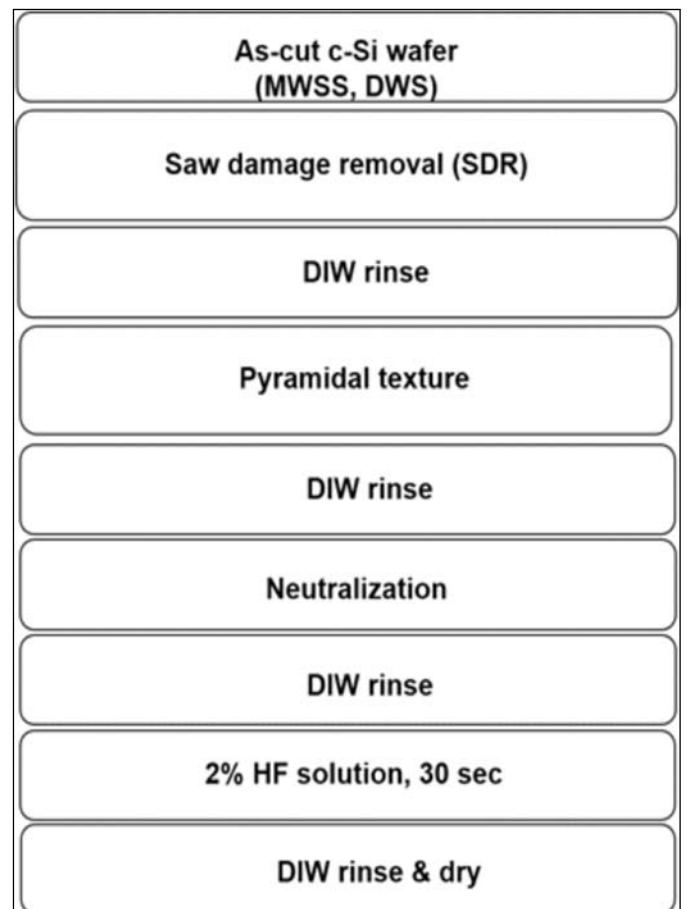


Fig. 4: Process flow diagram of the conventional alkaline texturing process

reaction across the complete Si wafer surface and in this way uniform texturing results.

As seen in Eqn. (1), a higher KOH concentration in the texturing solution results more H<sub>2</sub> and K<sub>2</sub>SiO<sub>3</sub> generation. More IPA is thus required to minimize the adverse effect of the H<sub>2</sub> bubbles. Also, the increased concentration of the K<sub>2</sub>SiO<sub>3</sub> as reaction by-product progressively slows down the Si etch rate [15] by the reduction of active KOH present

in the texture solution. Thus the Si-etching rate reduces rapidly leading to uncontrolled non-uniform pyramid formation marking the end-of-bath lifetime. Singh *et al.* [33] obtained maximum short circuit current for the cells fabricated using wafers with 35 minutes (min) texturing time with more than 2% KOH concentration (by weight). However, the same process bath cannot be repeatable for multiple batches (more than two) for the above reasons. Basu *et al.* [23] developed a low-IPA based texturing process by mixing an optimized amount of  $K_2SiO_3$  in the initial bath make-up of KOH (1.4% by weight). The initial quantity of silicate and a relatively low KOH concentration (as compared to the standard process) moderated Si etch rate to a large extent. Consequently the generation of  $H_2$  bubbles was reduced, in turn reduced the requirement for IPA. Also low silicate generation increases chemical bath stability. All these effects thus combine to perform texturing for c-Si surface covered with small and regular pyramids for a larger number of consecutive batches with little or no dosing of KOH, IPA and DIW into the texturing solution.

## 2.2 Group-2: Pyramidal texturing without KOH/NaOH

Several researchers have tried to replace KOH/NaOH based solutions with alternative chemical solutions. However, in these processes IPA is still essential for pyramid nucleation. Merloset *al.* [9] used tetra-methyl ammonium hydroxide (TMAH) in place of KOH as etch rates for TMAH/IPA solution is lower than those for KOH/IPA solution. They have used TMAH (25% by weight) mixed with IPA at 70-80°C temperature range for the formation of pyramidal Si surface. However, TMAH is comparatively a costly chemical as compared to KOH/NaOH and thus used only for specific applications. Tribasic sodium phosphate ( $Na_3PO_4 \cdot 12H_2O$ ) hydrolyzes in water. Due to its low dissociation constant, the concentration of hydroxyl ion ( $OH^-$ ) is very high in this solution [10]. Therefore,  $Na_3PO_4 \cdot 12H_2O$  solution was used for texturization of c-Si wafers.  $Na_3PO_4$  also plays the role of a surface active agent leading to the formation of pyramids with less IPA requirement as compared to NaOH texture bath. Hydrazine monohydrate ( $N_2H_4 \cdot H_2O$ ) was also applied [11] as the selective anisotropic etchant for pyramidal texturization. At higher temperature (90°C) hydrazine mono-hydrate breaks into ionized state and supplies  $OH^-$  which is essential for texturization. As per the literature, all these processes claim to generate uniform pyramidal surfaces. However, their applications in industries are not reported so far. Mainly, low-cost and easy availability of KOH/NaOH dominates for the industrial application.

## 2.3 Group-3: IPA-free Pyramidal texturing

Typical process bath temperature for texturing is  $\sim 80^\circ C$  and this temperature is near the boiling point of IPA. This way there is sufficient loss of IPA by evaporation during texturing which results in high IPA consumption. The high IPA usage is a significant cost, which in turn increases the cost per watt-peak of the solar cell. Therefore, elimination of IPA usage without detrimental impact on cell electrical performance, is always a key focus area for PV research.

Santana *et al.* [12] used low concentration of sodium carbonate/bicarbonate, i.e.,  $Na_2CO_3$  (1% by weight) /  $NaHCO_3$  (0.2% by weight), for texturization. This process also does not use IPA. However, to the best of our knowledge, till date there are no reports of cells with more than 18% efficiency for standard full-area aluminium back surface field large-area screen-printed solar cells using this pyramidal texturing process. It was shown by Lee *et al.* [13] that replacing IPA by chlorinated compound 2,4,6-trichloro-1,3,5-triazine to the NaOH solution generates an average reflectance of  $\sim 16\%$  over the 400-1100 nm wavelength range. The process time was longer (35 min) to result in undesirable larger pyramids of more than 7  $\mu m$  height. Sun and Tang [14] replaced NaOH by sodium hypochlorite ( $NaOCl$ ) as texturing chemical and the texturing lead to the formation of small pyramids with heights  $\sim 2 \mu m$ . This process uses ethyl alcohol (10% by volume) in place of IPA. Excellent low average reflectance of 10.8% over the 400-1000 nm wavelength range was also reported. However, higher cost of ethyl alcohol and safety issues make this process costlier and more hazardous for industrial use. Birman *et al.* [15] replaced IPA with 1,4 cyclohexanedial (CHX) for texturing. CHX has a higher boiling point (252°C) than IPA. Their recipe with a combination of KOH and CHX solution at 90°C generates small but uniform pyramid nucleation of  $\sim 2-4 \mu m$  pyramid height in just 10 min of texturing time. However, for industrial point of view, high cost of CHX is the main concern for its regular use. Wijekoon *et al.* [16] developed a new IPA-free chemical texturing process by employing polymer additives in aqueous KOH solution. The results had been validated with a number of repeated extended run production data. Mayer *et al.* [17] used aromatic organic substances, a micelles-forming agent, an aromatic acid, and a complex-forming agent, an aromatic alcohol, in KOH solution for texturing of c-Si wafer. The physical properties of new additives, especially their high boiling points and lower flammability compared to IPA generate a comfortable process window with higher process temperatures. The etch-rates of some solutions with these substances are with values above 1.2  $\mu m/min$  high enough for being used in inline texturing process. In the pilot-production a new texturing process based

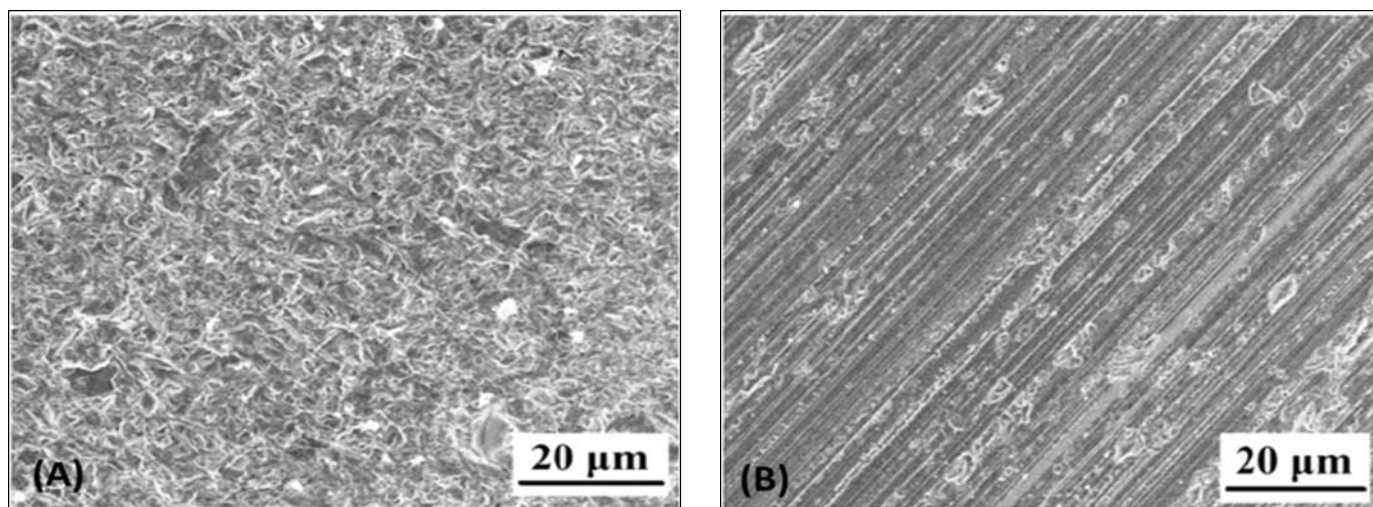


Fig. 5: SEM micrographs of the surfaces of (A) slurry-wire sawn (i.e., MWSS) wafer, and, (B) diamond-wire sawn (i.e., DWS) wafer [34]

on an aromatic acid as texturing additive reached the same texture qualities like the standard process in half the time [17]. Quiebraset *et al.* [18] textured c-Si wafers with an aqueous solution of KOH and a High Boiling Alcohol (HBA). When compared to IPA, HBA has less evaporation loss, cheaper (considering the quantity of the HBA used in the texturing bath and little redosing of the HBA in the texturing bath) and easier waste recycling. Equipment vendors like RENA GmbH [19] and Stangl GmbH [20] released commercial process tools for IPA-free texturing of monocrystalline silicon wafers. Some commercial chemical suppliers like Dow Chemical [21] and GP Solar [22] also released IPA-replacement additives. However, little detailed information has thus far been reported on these various technologies.

#### 2.4 Texturing process for the DWS c-Si wafers

Figure 5 shows the SEM images of the as-cut MWSS and DWS c-Si wafer surfaces [34]. The Si-surface in the MWSS wafer is heavily damaged as compared to the DWS wafer. Besides the DWS wafer have grooves generated during diamond wire sawing marks (Figure 4(B)). Therefore, the main concern of texturing is the effective SDR process just before the pyramidal texturing. An effective SDR process must etch the damaged Si-layer and also removes a-Si layer from the as-cut DWS c-Si wafer surface. After successful implementation of the effective SDR process, any standard alkaline texturing process can generate a low reflecting uniform pyramidal surface suitable for high efficiency cell fabrication.

Acid-based process using hydrofluoric (HF) – nitric (HNO<sub>3</sub>) [35,36] alkali-based processes using KOH/NaOH, TMAH [26] were tried to solve the above SDR related problems. Chen *et al.* [26] successfully reported a SDR

process with TMAH solution (25% by weight) at 85-90°C with an additional pre-SDR wafer clean step. This SDR process was followed by pyramid formation using NaOH solution mixed with commercial additive to achieve uniform pyramidal textured surface. Recently Basu *et al.* [28] developed a complete texturing process successfully by combining novel single step low-cost SDR solution with KOH and sodium hypochlorite (NaOCl), followed by pyramidal texturing using KOH, K<sub>2</sub>SiO<sub>3</sub> and IPA solution. The deep sawmarks along with a-Si layer over as-cut DWS surface were removed in the SDR process. This allows the formation of uniform smaller pyramids with ~2-4 μm height resulting a WAR of ~2.3% after application of conventional SiN<sub>x</sub> ARC layer. More importantly, this process uses low-cost chemicals as compared to the other SDR processes and can be used for multiple lots of wafers.

#### Conclusion

There are several approaches for the pyramidal texturing process for c-Si industrial wafers targeting cost reduction without compromising solar cell electrical performance. Small (~2-4 μm in height) but uniform pyramid formation is the ultimate target for everyone. Conventional process involves KOH/NaOH and IPA solution. However, researchers tried to replace KOH/NaOH with alternate chemicals, e.g., TMAH, tribasic sodium phosphate, hydrazine monohydrate, Na<sub>2</sub>CO<sub>3</sub>/NaHCO<sub>3</sub>, etc. Also, IPA is replaced by ethyl alcohol, HBA, CHX, commercial additives, etc. Key issues like high throughput and bath stability, safety, environmental impacts on chemical disposal, use of low-cost chemicals plays major role in deciding the optimized texturing process for any industry. Dominant use of DWS c-Si wafers now in PV industries makes the selection of alkaline texturing process more specific.

## Acknowledgement

This work was carried out at the National Centre for Photovoltaic Research and Education (funded by the Ministry of New and Renewable Energy, Government of India) under the project no.16MNRE002 at IIT Bombay.

## References:

1. E.D. Palik, O.J. Glembocki, I. Heard Jr., P.S. Burno, L. Tenerz, *J. Appl. Phys.*, **1991**, 70, 3291.
2. Q.B. Vu, D.A. Stricker, P.M. Zavracky, *J. Electrochem. Soc.*, **1996**, 143, 1372.
3. F. Restrepo, C.E. Backus, *IEEE Trans. Elec. Dev.*, **1976**, ED-23, 1193.
4. P. Verlinden, O. Evrard, E. Mazy, A. Crahay, *Sol. Energy Mater. Sol. Cells*, **1992**, 26, 71.
5. S.R. Chitre, *Proc. 13<sup>th</sup> IEEE PVSC*, **1978**, 152.
6. D.L. King, M.E. Buck, *Proc. 22<sup>nd</sup> IEEE PVSC*, **1991**, 303.
7. P.K. Basu, A. Khanna and Z. Hameiri, *Renewable Energy*, **2015**, 78, 590.
8. A. Khanna, P.K. Basu, A. Filipovic, V. Shanmugam, C. Schimiga, A.G. Aberle, T. Mueller, *Sol. Energy Mater. Sol. Cells*, **2015**, 132, 589.
9. A. Merlos, M. Acero, M.H. Bao, J. Bausells and J. Esteve, *Sensors and Actuators A*, **1993**, 37-38, 743.
10. U. Gangopadhyay, K.H. Kim, S.K. Dhungel, U. Manna, P.K. Basu, M. Banerjee, H. Saha, Junsin Yi, *Sol. Energy Mater. Sol. Cells*, **2006**, 90, 3557.
11. U. Gangopadhyay, K. Kim, S.K. Dhungel, P.K. Basu and J. Yi, *Renewable Energy*, **2006**, 31, 1906.
12. A.M. Santana, E. Rodriguez, B.G. Diaz, D. Borchert and R. Guerrero-Lemus, *Prog. Photovolt: Res. Appl.*, **2012**, 20, 191.
13. J. Lee, N. Lakshminarayan, S.K. Dhungel, K. Kim and J. Yi, *Sol. Energy Mater. Sol. Cells*, **2009**, 93, 256.
14. L. Sun and J. Tang, *Appl. Surf. Sc.*, **2009**, 255, 9301.
15. K. Birmann, M. Zimmer and J. Rentsch, *Proc. 23<sup>th</sup> EU PVSEC*, **2008**, 1608.
16. K. Wijekoon, T. Weedman, S. Paak, and K.M. Williams, *Proc. 35<sup>th</sup> IEEE PVSC*, **2010**, 3635.
17. K. Mayer, T. Orellana Pérez, M. Rostas, M. Schumann, F. Granek, S.W. Glunz, E. Rosenfeld, D. Kray and H. Antoniadis, *Proc. 25<sup>th</sup> EU PVSEC*, **2010**, 2511.
18. N.X. Quiebras, J. Junge, S. Seren, G. Hahn and E. Eppele, *Proc. 26<sup>th</sup> EU PVSEC*, **2011**, 849.
19. [http://www.rena.com/fileadmin/img/Produkte/200\\_Solartechnik/230\\_Batch/232\\_BatchTex/RENA\\_DB\\_monoTex\\_20110829\\_final.pdf](http://www.rena.com/fileadmin/img/Produkte/200_Solartechnik/230_Batch/232_BatchTex/RENA_DB_monoTex_20110829_final.pdf)
20. [http://www.stangl.de/uploads/tx\\_pspublications/MetaTex200\\_06.pdf](http://www.stangl.de/uploads/tx_pspublications/MetaTex200_06.pdf) [http://www.stangl.de/uploads/tx\\_pspublications/MetaTex200\\_06.pdf](http://www.stangl.de/uploads/tx_pspublications/MetaTex200_06.pdf)
21. M. Moynihan, C. O'Connor, B. Barr, S. Tiffany, W. Braun, G. Allardyce, J. Rentsch and K. Birmann, *Proc. 25<sup>th</sup> EU PVSEC*, **2010**, 1332.
22. <http://www.gpsolar.de/en/materials/chemicals/gp-alka-tex-zero/>
23. P.K. Basu, D. Sarangi, K.D. Shetty, and, M.B. Boreland, *Sol. Energy Mater. Sol. Cells*, **2013**, 113, 37.
24. H.J. Möller, C. Funke, M. Rinio, and, S. Scholz, *Adv. Eng. Mater.*, **2004**, 6, 501.
25. N. Watanabe, Y. Kondo, D. Ide, T. Matsuki, H. Takato, and, I. Sakata, *Prog. Photovolt: Res. Appl.*, **2010**, 18, 485.
26. K. Chen, Y. Liu, X. Wang, L. Zhang, and, X. Su, *Sol. Energy Mater. Sol. Cells*, **2015**, 133, 148.
27. C.W. Hardin, J. Qu, and, A.J. Shih, *Mater. Manuf. Process*, **2004**, 19, 355.
28. P.K. Basu, Sreejith KP, T.S. Yadav, A. Kottanthariyil and A.K. Sharma, *Sol. Energy Mater. Sol. Cells*, **2018**, 185, 406.
29. H. Nakaya, M. Nishida, Y. Takeda, S. Moriuchi, T. Tonegawa, T. Machida and T. Nunoi, *Sol. Energy Mater. Sol. Cells*, **1994**, 34, 219.
30. G. Willeke, H. Nussbaumer, H. Bender and E. Bucher, *Sol. Energy Mater. Sol. Cells*, **1992**, 26, 345.
31. J.D. Hylton, PhD Thesis, **2006**, University of Utrecht.
32. H. Seidel, L. Cespregi, A. Heuberger and H. Baumgartel, *J. Electrochem. Soc.*, **1990**, 139, 3612.
33. P.K. Singh, R. Kumar, M. Lal, S.N. Singh and B.K. Das, *Sol. Energy Mater. Sol. Cells*, **2001**, 70, 103.
34. X. Yu, P. Wang, X. Li and D. Yang, *Sol. Energy Mater. Sol. Cells*, **98** (2012), pp.337.
35. H. Park, S. Kwon, J.S. Lee, H.J. Lim, S. Yoon, and, D. Kim, *Sol. Energy Mater. Sol. Cells*, **2009**, 93, 1773.
36. J. Acker, T. Koschwitz, B. Meinel, R. Heinemann, and C. Blocks, *Energy Procedia*, **2013**, 38, 223.



Being among the toppers in National Entrance Test in Physics, **Dr. Prabir Kanti Basu** completed his Ph.D in 1997 from BITS, Pilani. During his Ph.D he worked on 'Crystalline Silicon Wafer Solar Cells' at National Physical Laboratory, New Delhi. In 1995 he started his career in semiconductor and solar industry. In 2003, he joined academics as Professor in engineering colleges in Faridabad and co-authored 5 books on Engineering Physics. In between, in 2004, he pursued advanced solar cell research at Sungkyunkwan University (SKKU), South Korea on sabbatical leave. Between 2010 to 2015 he was working at Solar Energy Research Institute of Singapore (SERIS), National University of Singapore (NUS) as Senior Research Scientist and Group Head on technology development of industrial high efficiency silicon wafer solar cells. This includes modified structures like selective emitter; passivated emitter and rear contact, etc., structures based on both tube and inline diffused emitters. Since 2016, he is working as Senior Project Executive Officer (Scientist), at NCPRE, IIT Bombay He is in-charge of complete solar cell fabrication line with research and development related to process and equipments. Till date he co-authored 34 international journals, 100 international conference papers and several international patents in areas of solar cells.



# Role of colloids and solvent chemistry in metal halide perovskites thin film and crystal formation.

**Pabitra K. Nayak**

*Clarendon Laboratory, University of Oxford, Parks Road, Oxford, OX1 3PU, UK  
E-mail: pabitra.nayak@physics.ox.ac.uk*

## Abstract

Metal halide perovskites (HaP) have emerged as a new class of soft semiconductor material. Despite the rapid progress in the device performances, reproducibility has been an issue. Thin films and single crystals of HaP are often prepared via solution route. The knowledge regarding the solvent chemistry, the composition of the precursor solution and their impact on the crystallization is necessary to reproduce/improve the electronic quality of the material. Many recent studies have shown that the acid-base equilibrium in solution affects the crystal growth. The presence of by-products (e.g., carboxylic acid) can change the onset of crystallization and also influence the thin-film morphology. By the addition of methyl amine, hydrohalic or carboxylic acids to the precursor solutions, the concentration of colloids can be tuned. Solutions with less colloidal particles give high quality of the thin films which in turn improves the optoelectronic device performances.

## Introduction

Metal halide perovskites (HaP) based optoelectronic devices have shown remarkable progress in last several years [1]. The ease of processing and the flexibility of varying the compositions have made these materials very attracting for optoelectronic applications. The power conversion efficiency (PCE) of solar cells prepared with HaP is now reaching 23% [2] which was around 9-10 % in 2012 [3,4]. Similarly, light emitting devices (LED) based on HaP as emitter also show promising efficiencies across the color gamut [5-8]. Highly efficient x-ray and gamma-ray detectors based on polycrystalline thin films and single crystals of HaP have also been demonstrated [9-13]. The progress of HaP based technologies has appeared as 'disruptive' compared to other thin film based optoelectronic devices. Many of the electronic properties (required for optoelectronic applications) @ of HaP are comparable to that of inorganic-based single crystalline GaAs though the preparation cost of the former is much lower [14]. Despite the rapid success of HaP materials in the optoelectronic device applications, there are many open questions about their fundamental properties. Single crystals are often treated as the best platform to evaluate the limits and possibilities of the semiconducting materials. Moreover, the crystallization process is also closely related to the thin film formation. Since thin-films of HaP materials are often prepared by solution routes, the chemical changes that happen in the precursor solution also affect the electronic quality of the thin film. Knowledge regarding the crystallization process and solvent chemistry is essential for the reproducibility, scalability and eventually commercial productions of HaP based devices.

In this mini-review, we discuss a mechanism of the rapid crystallization of the HaP materials from its precursor salt solution. We present how the solvent chemistry affects the crystallization processes. Different chemical species that forms in the precursor solvent influences the electronic properties of the thin films prepared. Manipulation of this solvent chemistry by adding suitable chemicals leads to better processing methods and material quality which is essential for highly efficient optoelectronic devices. We also discuss how colloidal particles present in the solution critically impact the electronic quality of the thin films.

## Metal Halide perovskites

Perovskite materials have a characteristic crystal structure same as that of  $\text{CaTiO}_3$ , often denoted as  $\text{ABX}_3$  (Figure 1 a, b). The metal halide perovskites have organic/ inorganic cations at the A sites, metal ions like  $\text{Pb}^{+2}$  and  $\text{Sn}^{+2}$  in the B sites and halides ( $\text{X}=\text{I}^-$ ,  $\text{Br}^-$ ,  $\text{Cl}^-$  or mixtures) at the X sites. Cations those frequently used at the A sites are methylammonium ( $\text{CH}_3\text{NH}_3^+$ ), formaminidium ( $\text{HC}(\text{NH}_2)_2^+$ ) and  $\text{Cs}^+$ . In figures 1a and 1b, we show schematic representations of the perovskite structure. Figure 1c and 1d show the schematics for the device architecture of perovskite-based solar cells. The films of HaP are deposited on top of an electron transporting or hole transporting material by spin-coating a precursor solution. The precursor solution is prepared by adding an adequate amount of the organic/ inorganic halide (e.g.,  $\text{CH}_3\text{NH}_3\text{I}$ ) and the metal halide (e.g.,  $\text{PbI}_2$ ) salts in an aprotic polar solvent (e.g., N-N dimethyl formamide).

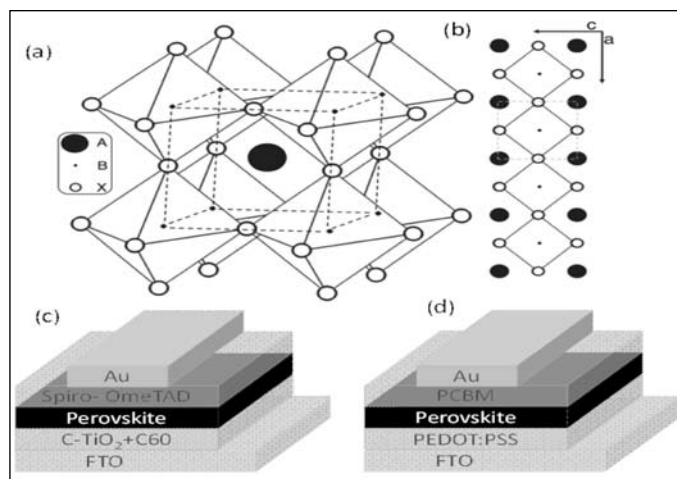


**Fig. 1:** (a) Schematic representation of perovskite structure  $ABX_3$  (b) Schematic illustration of the perovskite unit cell in 2D. (c) Typical device architectures of normal and (d) inverted perovskite solar cells, FTO = F doped Tin oxide, PCBM = Phenyl-C61-butyric acid methyl ester, PEDOT: PSS = poly(3,4-ethylenedioxythiophene) polystyrene sulfonate. Figure 1 (a) and (b) are adapted from ref. [4]

### Solvent chemistry and inverse solubility

Macroscopic HaP crystals can be prepared by a rapid crystallization route using “inverse solubility” [15] [16] effect. Since the nature of the rapid crystallization is closely related to the crystallization of perovskites in thin films a detailed understanding of the mechanism enables the progress in quality and reproducibility of both single crystals and thin films for optoelectronic device applications.

Solubility is a thermodynamic property for a given salt-solvent system. For a given concentration of salts, the saturation that leads to crystal formation should happen at the same temperature at every attempt. However, it is observed that the time and temperature required for crystallization of metal halide perovskites depend on the history of the solvents, dimethylformamide (DMF) or  $\gamma$ -butyrolactone (GBL)). Moreover, for a given temperature, different saturation concentrations have been reported for the same salt-solvent system. This observation indicated that many other factors modulate the inverse solubility effect in addition to the simple ionic solubility consideration, by which saturation happens.

DMF can decompose into formic acid (FAH), and dimethylamine (DMA) and GBL can decompose to  $\gamma$ -hydroxybutyric acid (GHB) over time. Both formic acid and  $\gamma$ -hydroxybutyric acid are carboxylic acids. The authors in the ref. [17] hypothesized that the carboxylic acids (by-products of the solvent degradation), independent of temperature, could induce the crystallization of organic-inorganic halide perovskites, in DMF with the addition of

FAH, and in GBL with the addition of GHB. The authors began replicating the systems as previously reported, a 1M solution of bromide salts ( $CH_3NH_3Br$  and  $PbBr_2$ ) in DMF and iodide salts ( $CH_3NH_3I$  and  $PbI_2$ ) in GBL, but with temperatures  $\sim 25\text{-}30^\circ\text{C}$  lower than those required for crystallization in the prior reports. Under these conditions, they did not observe any crystallization, even after several hours of heating. When they added FAH to the DMF and GHB to the GBL, and they observed that crystallization within 5 minutes which indicated that the by-products of the degradation do influence the crystallization. The authors showed that it is possible to systematically reduce the onset of the crystallization by adding a carboxylic acid (e.g., formic acid to the bromide salts in DMF) to the salt solution. The addition of carboxylic acid to perovskite precursor solutions also helped to induce the crystals in many other solvent systems.

The degradation of solvents is an irreversible process while the inverse solubility is reversible with temperature. The degradation of solvents cannot alone explain the observed inverse solubility effect. To probe the inverse solubility process further, the authors used in-situ ATR measurements on the solutions in the presence and absence of carboxylic acids. They found that the organic salt, methylammonium ( $MAH^+$ ) which is also a weak acid dissociates more into its conjugate base methylamine (MA), and the dissociation is suppressed in the presence of the carboxylic acids. The increased amount of MA in the solvent system increases the solubility of perovskite material in the solvent system. The presence of a carboxylic acid which is a stronger acid than  $MAH^+$  reverses the dissociation of  $MAH^+$ , i.e., more  $MAH^+$  produced from the association of  $H^+$  with the MA present in the solvent system. The reduction of MA in the solvent system decreases the overall solubility of perovskite materials. Plausible acid-base equilibria are shown in equation 1.



where  $w$ ,  $x$ ,  $y$ , and  $z$  are undetermined stoichiometric coefficients, FAH= formic acid

### Role of colloids

The precursor solutions of HaP in solvents like DMF or GBL do not have only the solvated ionic species; they also have colloidal particles in them.

The scattering of laser light due to the presence of colloids can be observed by passing a beam laser light

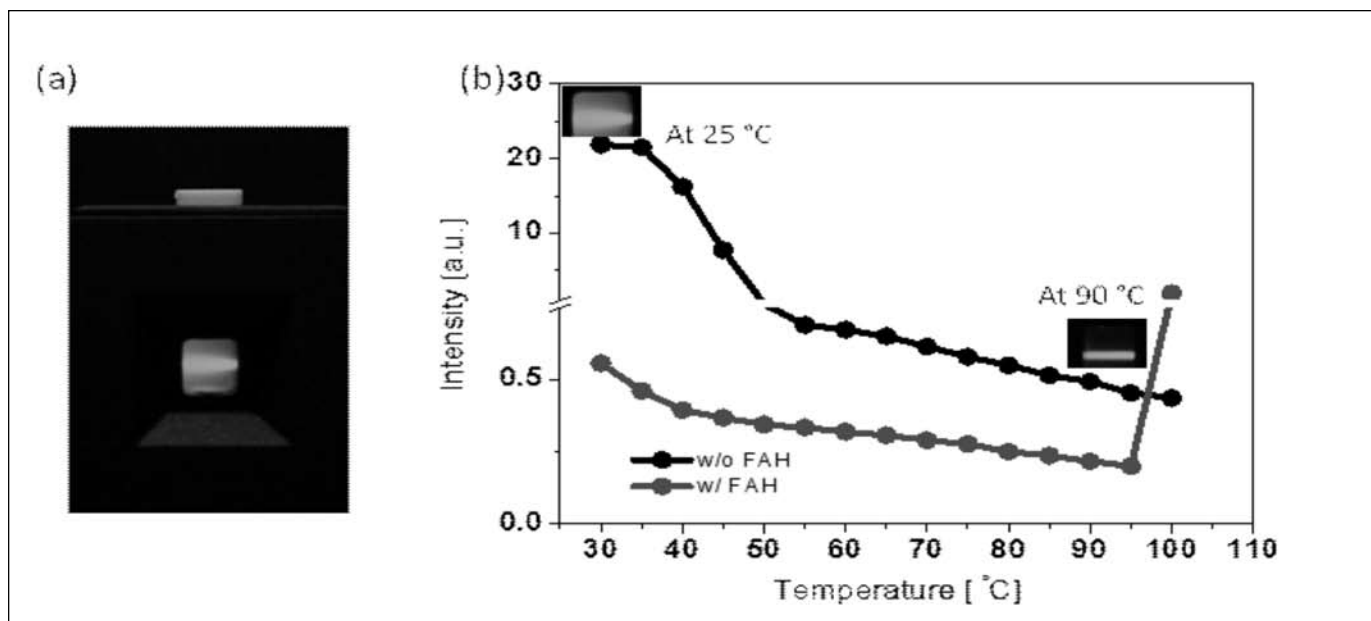


Fig. 2: (a) Optical photograph of a cuvette containing 1M (MAI + PbI<sub>2</sub>) in GBL with a laser light beam (532 nm) passing through the solution. (b) Static light scattering at different temperatures with and without formic acid.

through a saturated HaP precursor solution (See Figure 2a).

When the authors removed some of the colloids from the solution, the onset, as well as the yield of the crystals, were affected. To understand how these colloids influence the crystallization, they authors performed static light scattering measurements (Figure 2 b) and interferometric scattering microscopy (iSCAT) measurements. They found that the size/number of the colloids decreased with the increase in the temperature. The presence of carboxylic acid facilitates the breaking of the colloids. Based on the in-situ ATR-IR measurements, static light scattering measurement, iscat measurements the authors proposed a mechanism as illustrated in figure 3.

Briefly, some part of the ionic constituents is stored in colloidal particles at the beginning. With the increase in the temperature, the proton concentration in the solution increases. Both higher temperature and proton concentration break the colloidal particles releasing more ions into the solution. The excess ions in the solution cause supersaturation and thus the crystallization. The fact that CsPbBr<sub>3</sub> crystal formation can happen in DMSO via inverse solubility, the change in the acid-base equilibrium is not a sufficient condition for inverse solubility.

### Role of colloids in thin films formation

While the colloids act as reservoirs in 'inverse solubility' method for the single crystal growth, their presence also has a direct link between the nucleation and crystal growth

in polycrystalline thin films preparation. McMeekin et al. [18] have shown that these colloids provide nucleation sites for the crystal growth which in turn impacts the morphology, crystalline quality, and the optoelectronic properties. The authors found that the addition of HI and HBr to the precursor solution decreases the concentration of colloidal particle present in the solvent system. A lower concentration of colloids is essential to get highly ordered and textured crystalline film for [HC(NH<sub>2</sub>)<sub>2</sub>]<sub>0.83</sub>Cs<sub>0.17</sub>Pb(Br<sub>0.2</sub>I<sub>0.8</sub>).

### Impact of methylamine in the solution

From the discussions in the previous section, it can be inferred that the presence of methyl amine can increase the solubility of the perovskite material in a solution. Highly efficient perovskite cells prepared via the precursor solution route often use polar aprotic solvents like DMF, GBL, DMSO and the mixture of these solvents. The choice of the solvent is many times limited by the solubility of the Pb salts. Moreover, the toxicology concern of highly coordinating solvents like DMF which is commonly used for perovskite solar cell preparation poses a barrier for the large-scale fabrication of the devices. Moreover, it is also needed prolonged annealing period to remove the solvents from the thin film. To circumvent this problem, Noel et al. [19] have used a mixture of MA and Acetonitrile (ACN) as a solvent to prepare the precursor solution of perovskite. ACN alone is a non-solvent for MAPbI<sub>3</sub>. However, its mixture with MA is a very potent solvent for MAPbI<sub>3</sub>. ACN is a low viscous and low boiling solvent. The rapid

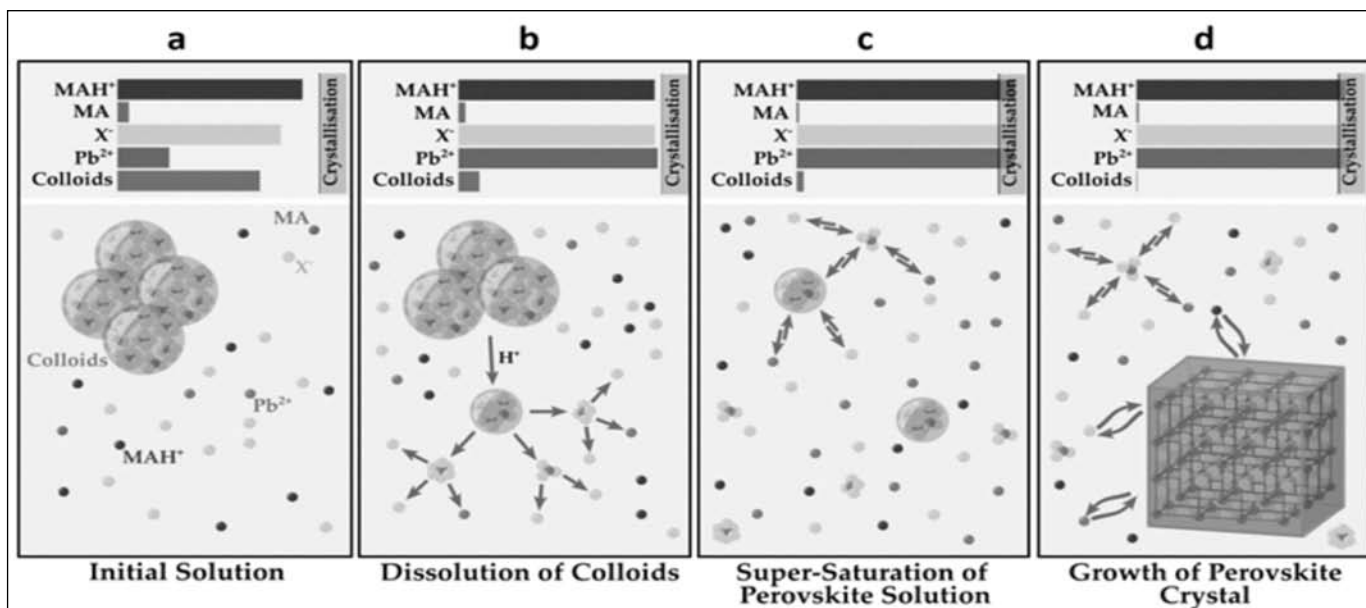


**Fig. 3:** Schematic of the crystallization mechanism: Concentration of Pb<sup>2+</sup>, X<sup>-</sup>, MAH<sup>+</sup>, MA and colloids (not to scale) are represented by the horizontal bars on the top of each panel. Spheres with similar color schematically represent each species in the bottom panel. The regime for crystallization is represented by the vertical bar in the top panel. (Figure is adapted from ref [17] with permission © Nature Publishing Group)

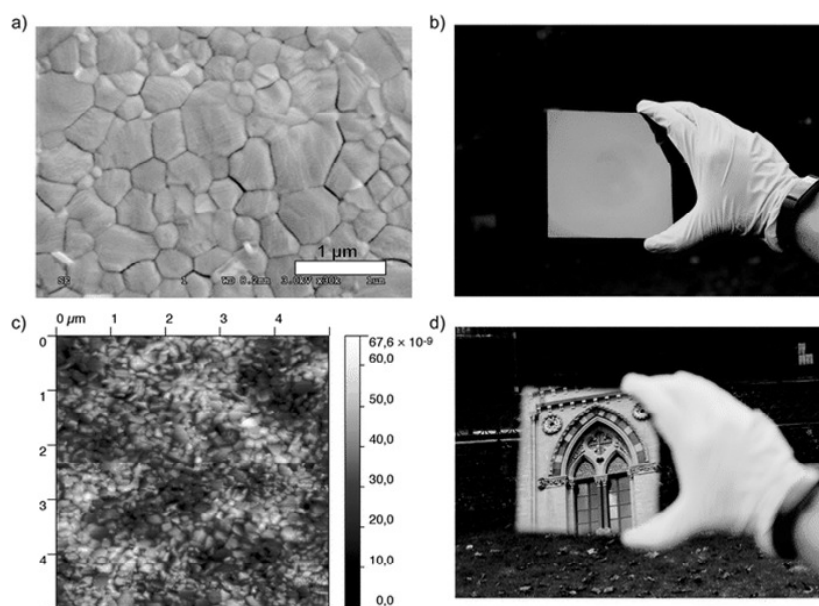


**Fig. 4:** SEM image of the top surface of a poly-crystalline film of CH<sub>3</sub>NH<sub>3</sub>PbI<sub>3</sub> prepared by ACN+MA solution. (c) AFM image of the film (area = 5 μm × 5 μm) (b) and (d) Photographs of a 125 cm<sup>2</sup>, highly specular, the pinhole-free film deposited via spin coating from a precursor of CH<sub>3</sub>NH<sub>3</sub>PbI<sub>3</sub> in ACN+MA solvent. (The figure is adapted from ref. [19] with permission© Royal Society of Chemistry).

evaporation of ACN and MA mixture during spin coating process at the room temperature gives a very uniform film of MAPbI<sub>3</sub> over an area as large as 125 cm<sup>2</sup>.

The average grain size in the polycrystalline film prepared by this method is several hundred nanometres which are higher than what is generally observed in other rapid crystallization methods such as anti-solvent

quenching method. The material quality is also higher than the thinfilms prepared by other single step spin-coating method which is reflected in higher photoluminescence lifetimes. The surface roughness of the films prepared via the ACN+MA route is also three times lower than the films prepared by the conventional 1 step spin-coated films.

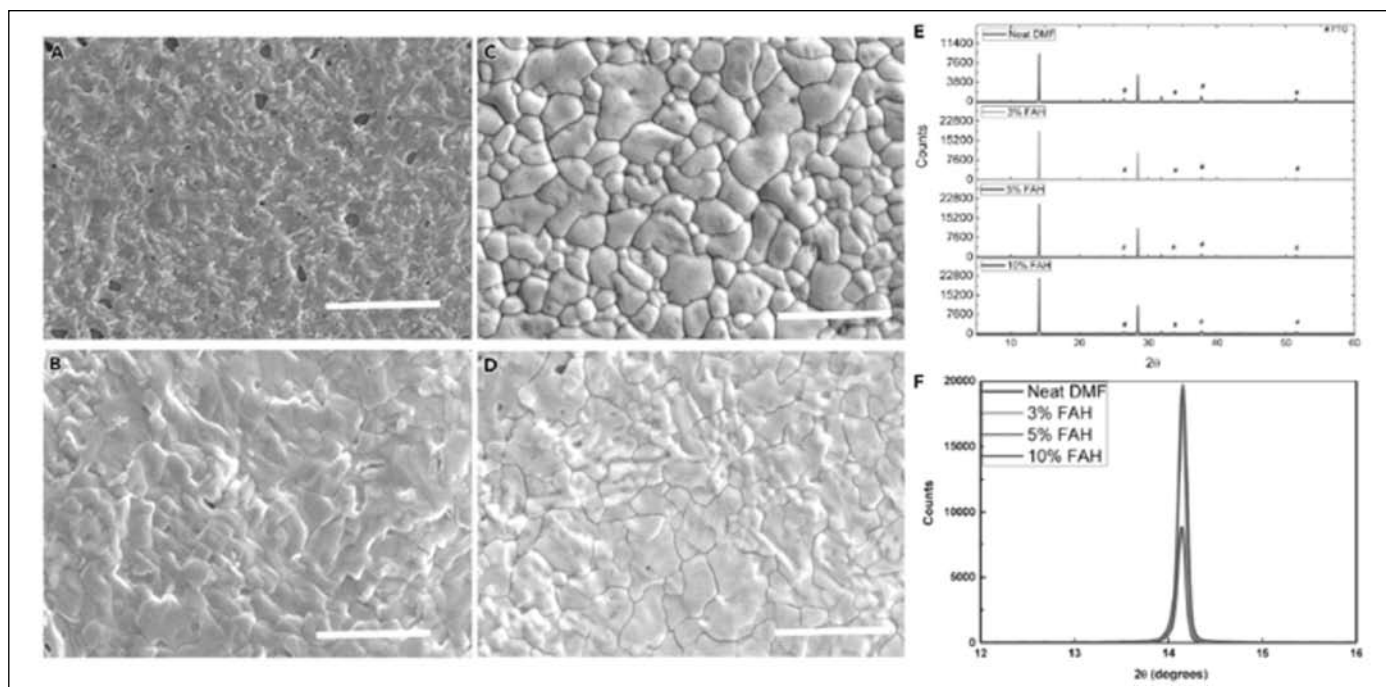


**Figure 5:** (a) SEM images of perovskite films ( $\text{MAPbI}_{3-x}\text{Cl}_x$ ) coated from neat DMF and with added formic acid (A) neat, (B) 3 vol %, (C) 5 vol %, and (D) 10 vol %, scale bar  $5\mu\text{m}$  (E) XRD of thinfilms prepared from neat and acidified solvent systems. (F) 110 peak of the perovskite films shown in (E). Adapted from ref. [22] with permission. © Cell Press

The highly uniform film seen in these cases is possible because  $\text{CH}_3\text{NH}_3\text{PbI}_3$  precursor solution in ACN+MA has hardly any colloidal particles in it. Rapid crystallization happens with very low nucleus sites which give micron scale grains (Fig. 4a) with better electronic properties. Perovskite Solar cells with normal and inverted architecture with thin films prepared via ACN+MA route showed PCE 17-18%.

### Formic acid as performance booster

Addition of formic acid to the crystal growth solution is known to improve the electronic quality of the single crystals [20]. Noel et al. have shown that the addition of formic acid to the precursor solution in DMF boost the device performance [21]. The change in the pH of the precursor solvent that happens due to the degradation of DMF correlates with the change in the colloid concentration in the solution. Addition of formic acid to the solution catalyzes the degradation of the solvent. The degradation products, mainly dimethyl amine dissolves the colloids. Like the previous case, here also the precursor solutions with a lesser amount of colloids gave better quality films and thus higher performance. Figure 5 shows the impact of added formic acid on the morphology of the films.

### Conclusion and outlook

The solvents used for the preparation of the precursor solutions undergo degradation over time. As the

degradation happens in an uncontrolled manner, the amount of degradation products in the solvent system is not a constant. Since the degradation products have an impact on the formation of crystals and thin film, the inconsistency in their number affects the reproducibility in the preparation of thin film and crystals. Presence of carboxylic acids in the precursor solution decreases the onset of the crystal formation. Colloidal particles are present in the precursor solutions. These particles influence the crystallization process of perovskites. Colloidal particles act as seeds for the crystal growth during thin-film formation, hence a very small amount is needed to grow thin films with large grains. A lesser number of colloidal particles in the solution correlates with better electronic quality films. The number of colloidal particles in solution can be reduced by the direct addition of methyl amine or by the generation of amines through the degradation of the solution. We have discussed here the influence of the solvent and colloids on the Pb based perovskite systems. The influence of solvent systems on mixed metal ions (e.g.,  $\text{Pb}^{+2}$  and  $\text{Sn}^{+2}$ ) is expected to be more severe as the degradation product can act like oxidant/ reductant which will control the ratio of  $\text{Sn}^{+2}$ :  $\text{Sn}^{+4}$  in the precursor solution. Moreover, the compositional variation in the colloids can lead to inhomogeneity in the film property which will have

a huge impact on the device performance and stability. Better knowledge of the solvent-solute interactions and suppression/control of degradation in solvents will help to improve reproducibility and hence the scalability of perovskite-based devices.

### Acknowledgment

The author acknowledges the support from the EPSRC, UK. The author thanks Dr. B. Wenger (University of Oxford) for providing dynamic light scattering data on perovskite precursor solutions.

### References:

1. M. A. Green, A. Ho-Baillie, H. J. Snaith, *Nat. Photonics* **2014**, 8, 506–514.
2. M. A. Green, Y. Hishikawa, E. D. Dunlop, D. H. Levi, J. Hohl-Ebinger, A. W. Y. Ho-Baillie, *Prog. Photovoltaics Res. Appl.* **2018**, 26, 3–12.
3. H.-S. Kim, C.-R. Lee, J.-H. Im, K.-B. Lee, T. Moehl, A. Marchioro, S.-J. Moon, R. Humphry-Baker, J.-H. Yum, J. E. Moser, et al., *Sci. Rep.* **2012**, 2, 591.
4. M. M. Lee, J. Teuscher, T. Miyasaka, T. N. Murakami, H. J. Snaith, *Science* **2012**, 338, 643–7.
5. S. D. Stranks, H. J. Snaith, *Nat. Nanotechnol.* **2015**, 10, 391–402.
6. M. Yuan, L. N. Quan, R. Comin, G. Walters, R. Sabatini, O. Voznyy, S. Hoogland, Y. Zhao, E. M. Beauregard, P. Kanjanaboos, et al., *Nat. Nanotechnol.* **2016**, 11, 872–877.
7. N. Wang, L. Cheng, R. Ge, S. Zhang, Y. Miao, W. Zou, C. Yi, Y. Sun, Y. Cao, R. Yang, et al., *Nat. Photonics* **2016**, 10, 699–704.
8. N. K. Kumawat, D. Gupta, D. Kabra, *Energy Technol.* **2017**, 5, 1734–1749.
9. Y. C. Kim, K. H. Kim, D.-Y. Son, D.-N. Jeong, J.-Y. Seo, Y. S. Choi, I. T. Han, S. Y. Lee, N.-G. Park, *Nature* **2017**, 550, 87–91.
10. H. Wei, Y. Fang, P. Mulligan, W. Chuirazzi, H.-H. Fang, C. Wang, B. R. Ecker, Y. Gao, M. A. Loi, L. Cao, et al., *Nat. Photonics* **2016**, 10, 333–339.
11. S. Shrestha, R. Fischer, G. J. Matt, P. Feldner, T. Michel, A. Osvet, I. Levchuk, B. Merle, S. Golkar, H. Chen, et al., *Nat. Photonics* **2017**, 11, 436–440.
12. H. Wei, D. DeSantis, W. Wei, Y. Deng, D. Guo, T. J. Savenije, L. Cao, J. Huang, *Nat. Mater.* **2017**, 16, 826–833.
13. S. Yakunin, D. N. Dirin, Y. Shynkarenko, V. Morad, I. Cherniukh, O. Nazarenko, D. Kreil, T. Nauser, M. V. Kovalenko, *Nat. Photonics* **2016**, 10, 585–589.
14. T. M. Brenner, D. A. Egger, L. Kronik, G. Hodes, D. Cahen, *Nat. Rev. Mater.* **2016**, 1, 15007.
15. M. I. Saidaminov, A. L. Abdelhady, B. Murali, E. Alarousu, V. M. Burlakov, W. Peng, I. Dursun, L. Wang, Y. He, G. Maculan, et al., *Nat. Commun.* **2015**, 6, 7586.
16. J. M. Kadro, K. Nonomura, D. Gachet, M. Grätzel, A. Hagfeldt, *Sci. Rep.* **2015**, 5, 11654.
17. P. K. Nayak, D. T. Moore, B. Wenger, S. Nayak, A. A. Haghighirad, A. Fineberg, N. K. Noel, O. G. Reid, G. Rumbles, P. Kukura, et al., *Nat. Commun.* **2016**, 7, 13303.
18. D. P. McMeekin, Z. Wang, W. Rehman, F. Pulvirenti, J. B. Patel, N. K. Noel, M. B. Johnston, S. R. Marder, L. M. Herz, H. J. Snaith, *Adv. Mater.* **2017**, 29, 1607039.
19. N. K. Noel, S. N. Habisreutinger, B. Wenger, M. T. Klug, M. T. Horantner, M. B. Johnston, R. J. Nicholas, D. T. Moore, H. J. Snaith, *Energy Environ. Sci.* **2017**, 10, 145–152.
20. Q. Lv, Z. Lian, Q. Li, J.-L. Sun, Q. Yan, *Chem. Commun.* **2018**, DOI 10.1039/C7CC07154J.
21. N. K. Noel, M. Congiu, A. J. Ramadan, S. Fearn, D. P. McMeekin, J. B. Patel, M. B. Johnston, B. Wenger, H. J. Snaith, *Joule* **2017**, 1, 328–343.
22. N. K. Noel, M. Congiu, A. J. Ramadan, M. B. Johnston, B. Wenger, H. J. Snaith, **2017**, DOI 10.1016/j.joule.2017.09.009.



**Pabitra K. Nayak** received his Ph.D. from the Tata Institute of Fundamental Research, Mumbai, India. He then worked as a postdoctoral fellow at the Weizmann Institute of Science, Israel. He is currently at the University of Oxford, where his research interests involve the development of new materials for optoelectronic applications and understanding the chemistry that controls the electronic properties of halide perovskites

# Controlling Nucleation and Growth to Engineer Nanocrystal Composition and Morphology

Rekha Mahadevu, Dev Kumar Thapa, Biswajit Bhattacharyya and Anshu Pandey<sup>1,\*</sup>

<sup>1</sup>Solid State and Structural Chemistry Unit, Indian Institute of Science, Bangalore-560012

\*E-mail: anshup@iisc.ac.in

## Abstract

We describe the recent progress made in terms of controlling nucleation and growth steps in colloidal syntheses. This review emphasizes three variants of conventional colloidal synthesis, where control over nucleation is employed to regulate material monodispersity, composition and morphology respectively. Some of these schemes in particular represent departures from the conventional nucleation-growth-ripening paradigm, and thus offer interesting new routes to making colloidal materials.

## Introduction

Nanomaterials have been attractive materials in field of science as well as technology from the past half century, with a host of promising applications ranging from electronic devices [1-7] to fluorescent markers for biological imaging [8-10]. With the advent of colloidal synthesis, the simultaneous formation of large numbers of nanoparticles became feasible. This shifted the emphasis of the nanoscience effort towards catering to applications of scale such as photovoltaics, lighting and displays. Most of these applications require a high quality of sample in copious quantities. Thus within colloidal synthesis itself, an enormous effort had been devoted to improve the quality of nanoparticles as well as to enable the scaling up of reactions [11-15].

In any colloidal synthesis, the nanocrystal (NC) formation occurs through two major steps, a nucleation event that is followed by growth. During the growth phase, most reactions employ some form of a size focusing approach that eventually leads to narrow size dispersion. Such growth regimes are mostly understood to be variants of the Ostwald ripening phenomenon. In certain specific cases, researchers have employed alternate strategies such as digestive ripening [16-18] that improve particle size distribution as a post-synthetic modification. However such strategies are ill-suited except in the case of the simplest of materials. In order to achieve more complex materials, it becomes necessary to eliminate the ripening phases of growth altogether, and rather achieve synthetic conditions where monodispersity may be achieved without resorting to conditions amenable to ripening. In this situation, it is necessary to ensure the homogenous growth over the entire synthesis. This is achieved by maintaining synthetic conditions where the nucleation step is a well-resolved single event and growth conditions do not allow

for secondary nucleation steps. This is usually done in most synthesis by causing the super saturation of the precursors at the initial stages to force nucleation [19-21]. Subsequently, growth steps occur slowly from solutions with substantially reduced precursor concentrations. While these steps have been explored by several workers in literature, [12, 21-23] and are described in numerous articles, we will cover certain variants of these basic steps that have been developed in our laboratory. These methods have been devised to address three specific challenges. Firstly, we introduce a nucleation-growth mechanism for lead chalcogenides that can be beneficial in ensuring the scaling up of their synthesis. Next, we turn our attention to the NC doping problem, where a new nucleation-growth strategy is introduced to explore the concentrated doping limit (>30%). Finally we will explore a method to produce nuclei within a shaped template to enable the synthesis of shape controlled materials.

## Separating Nucleation and Growth via an Anion Exchange Reaction [11]

Synthesis of lead chalcogenides nanoparticles is well known in literature, [24-29] and has been the subject of numerous reports. Lead chalcogenides are important materials for near infrared to mid infrared (NIR-MIR) optoelectronics and their NCs are suitable candidates for several applications [30-31]. However, the lack of understanding about the reaction mechanism has complicated the large scale synthesis of these materials, besides creating uncertainties in reaction yields, irregular shapes and polydispersity.

PbSe NCs were synthesized by following procedure in the literature [26]. The first step of the conventional PbSe synthesis involves conversion of lead salts into lead oleate by heating lead salts with oleic acid and 1-octadecene (ODE) under inert condition. Then selenium dissolved

in trioctylphosphine (TOP) was injected into pre formed lead oleate. In 2006 Steckel *et.al* [32] first time proposed the mechanism for PbSe NCs formation. In this article the authors proposed that there are two steps involved in the reaction mechanism.

In first step as soon as TOPSe is injected into preformed lead oleate, selenium from TOP=Se attacks  $Pb(OOR)_2$  and forms  $ROO-Pb--Se=TOP$ , gives PbSe monomers. In second step, the  $PH(OR_2)$  suspected dioctyle phosphine oxide (DOP) which is present in technical grade of TOP has an impurity attacks  $Pb(OOR)_2$  and reduces  $Pb^{2+}$  to  $Pb^0$ , then this  $Pb^0$  attacks Se of TOPSe and oxidises  $Se^{2-}$  to  $Se^0$  and form PbSe monomers. Once these monomers exceeds solubility limit, they combine together and nucleates PbSe NCs as well as growth step of the reaction.

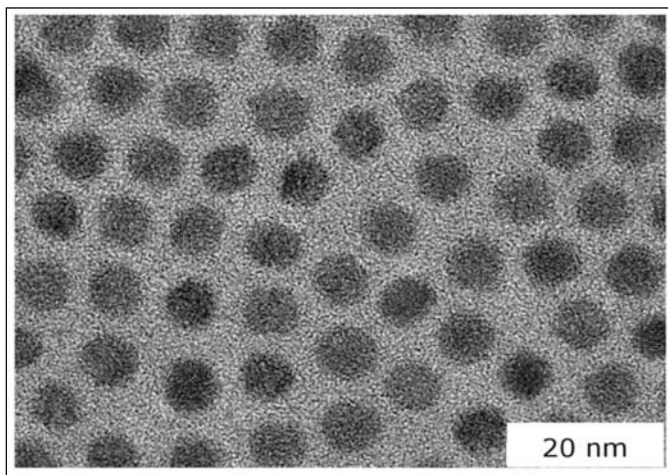


Fig. 1: TEM image of PbSe based NCs synthesized using lead oleate prepared from lead oxide [11]

A further study on PbSe was done by Joo *et al.* [28]. They also demonstrated the effect of dialkylphosphine impurities on the quantum yield of the PbSe NCs. In this work they used 1, 2-hexadecanediol (HDD) as a surrogate reducing agent instead of DOP because DOP acts as surface traps and results low quantum yield of NCs.

It has been shown that PbSe NCs (Figure 1) synthesized by using two different lead precursors, lead to drastic variation in material quality. In these experiments, other reaction conditions and precursor were kept constant in both the cases. However the optical absorption spectrum of the PbSe NCs synthesized using lead acetate and lead oleate source have long tail, extended up to near IR regions. This tail indicates that there is bad size distribution (Figure 2). The PbSe NCs synthesized by using lead oxide as lead precursor have sharp exciton (and a good size dispersion (Figure 1)). This sharp spectral feature in the optical absorption spectra indicates that, there is good size

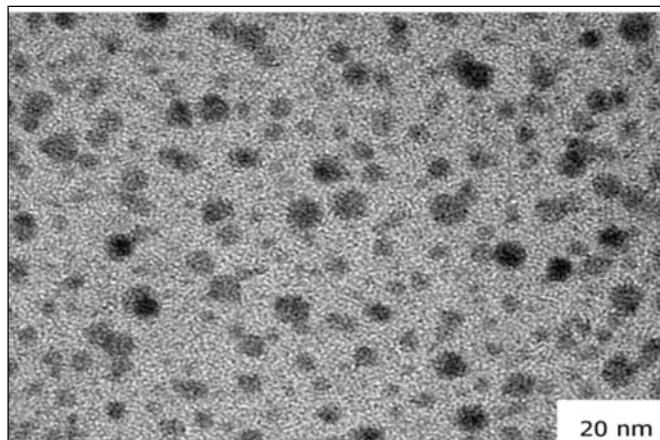


Fig. 2: TEM image of PbSe based NCs synthesized using lead oleate prepared from lead acetate [11].

distribution of the PbSe NCs. If the reaction follows the above conventional mechanism both the lead precursors should give same quality of PbSe NCs. From the above results it was concluded that, the lead oleate obtained from two different lead sources have some role in the formation of PbSe NCs.

To resolve this issue further, lead oleate precursors were analysed before adding TOPSe. While lead oleate prepared out of lead acetate absorbs no light in the visible region of the spectrum, the conventionally prepared lead oleate is found to have a yellowish tinge. Further investigation showed this to be related to be the absorption of lead oxide nanoparticles.

It was hypothesized that annealing of lead oxide at 150 °C with oleic acid and ODE gives lead oxide nanoparticles. These PbO nanoparticles exchange their anion with Se of TOPSe results PbSe that represents an anion exchange reaction. To prove the above hypothesis yellow lead oxide nanoparticles were prepared and then TOPSe was injected into these preformed PbO nanoparticles at room temperature (RT), after 30 minutes the solution turned to brown. It was shown that the XRD pattern of PbO changes upon addition of TOPSe. In particular, after addition of TOPSe the XRD pattern matches with the standard XRD pattern of PbSe. The above experimental observation suggests that there are two steps involved in the reaction path. One is anion exchange reaction and other one is growth.

In the anion exchange reaction the lead oxide NCs which are present in the lead oleate precursor, exchanges there oxygen with selenium. This exchange happens because  $Pb^{2+}$  ions are nearly neutral Lewis acids and thus they have more affinity towards soft  $Se^{2-}$  Lewis bases compared to  $O^{2-}$  ligands which are hard. On the other



hand the enthalpy of formation of PbSe (-100KJ/mol, theoretical data) [33] is higher than enthalpy of formation of PbO (-219 KJ/mol, theoretical data) [34], implying that the direct exchange is likely to be thermodynamically not feasible. The other factor which contributes to the feasibility of the anion exchange reaction is affinity of phosphorous towards oxygen compare to selenium. As soon as the TOPSe is injected into the flask containing PbO nanoparticles which are formed out of lead oleate by decarboxylation, [35-36] it undergoes anion exchange reaction with PbO nanoparticles forms TOPO and PbSe. The growth step the lead oleate and selenium reaction follows a reductive path way, which was proposed by Steckel *et.al*, [32] and deposited on PbSe nuclei.

To understand this further the reaction was started with variously prepared lead oleate. Initially, lead acetate was converted into lead oleate by heating with oleic acid at 100 °C. Note that at this temperature lead oxide nanoparticle does not form. Then this was divided into 3 equal parts. TOPSe added into one part as such without further treatment. The second part was heated to 180 °C, then TOPSe was added. The third part was treated with NaOH then TOPSe was added. All three cases gives PbSe NCs with different quality, that reflects the different nucleation and reaction kinetics which again depend on the quality of PbO formed in the previous steps [11].

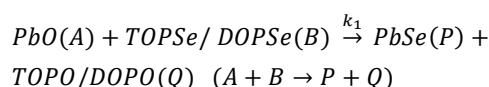
Annealing at 180°C and the addition of a strong alkali again leads to the partial conversion of lead oleate into PbO. The resultant solution is then treated with TOPSe lead to high quality PbSe MSNCs (Magic Sized Nanocrystals).

The reason behind the existence of this correlation was inferred from the reaction kinetics that was observed in differently treated lead oleate solutions. In this experiment, one fraction of lead oleate was treated with sodium hydroxide, another was annealed, while the third was only exposed to low (100 °C) temperatures in its preparation history. Thus, the former two solutions are contaminated with PbO particles, while the latter is pure lead oleate. Then the lead oleate stock solution was treated with equal quantities of TOPSe at room temperature [37]. After some time has passed ( $10^5$  s), it was shown that all three solutions roughly absorb same amounts of light at 400 nm region, suggesting equal quantities of PbSe formation in all three conditions. This suggests that PbO does not control the total amount of PbSe produced in the reaction, but plays an important role in controlling monodispersity and quality of NCs [11].

Even though all three reactions finish roughly at same timescales, the presence of PbO influences the nucleation steps of the reaction. In particular, the kinetics indicated

that there is no PbSe produced within the reaction mixture until 1000 s and other two cases where PbO NCs are present indicate the formation of PbSe well before 1000 s. Thus, in both reactions PbSe is already produced within the first 100 s of addition of TOPSe. The difference in the early time reaction of the two types of reactions suggests that PbO is involved in the nucleation of PbSe NCs. The kinetics also explains the correlation between monodispersity and the presence of PbO. In absence of PbO NCs, the nucleation process itself is delayed (PbSe formation is observed as late as 2000 s after the TOPSe addition). The absence of a single, clear nucleation event gives rise to a poor size dispersion.

The reaction scheme is thus summarized:



Rate of formation of PbSe is dependent on the concentration of PbO nanoparticles and TOPSe/DOPSe.

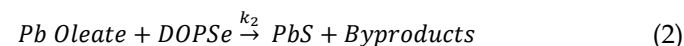
Therefore,  $\frac{dP}{dt} = k_1AB$ , starting with the assumption of first order kinetics. A is unity because PbO is in the solid form during the initial reaction time and it drops to zero during its consumption and then the reaction terminates instantaneously. So, is taken as 1, leading to

$$\frac{dP}{dt} = k_1AB \quad (1)$$

Following this, one obtains the rate expression,

$$P = B_0 [1 - e^{-k_1t}]$$

The growth step involves deposition of PbSe:



PbSe NCs grow by the deposition of PbSe on top of existing PbSe nuclei. In general, surface catalyzed/surface deposition reactions usually exhibit a zero order. In particular, for the reaction studied here, the rate determining step would be a reactive collision of Pb Oleate and TOPSe on the surface of a PbSe QD. This is clearly independent of reagent concentrations over a broad range. This suggests that growth step follows zero order kinetics. We thus write the consolidated expression, assuming  $k_2 \ll k_1$ ,

$$P(t) = \begin{matrix} B_0 [1 - e^{-k_1t}] & \text{Before Exhaustion of PbO} \\ k_2t & \text{After Exhaustion of PbO} \end{matrix} \quad (3)$$

Within the noise in the experimental data, it was not possible to determine the reaction orders particularly for the second step with complete certainty. The excellent

agreement between the observed and predicted trend however suggests a small or near vanishing reaction order.

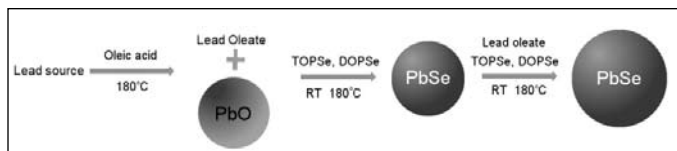


Fig. 3: Scheme of PbSe formation using an anion exchange mediated nucleation

The time versus change in volume of NCs clearly showed a multi-step behavior whereby the nucleation occurs via a very rapid anion exchange, while the growth takes place through a slower ordinary reaction scheme. The role of anion exchange in ensuring a single nucleation step is thus established [11].

### Accessing concentrated regimes of doping through kinetic control [38]

As shown above, advanced colloidal chemistry has enabled the synthesis of semiconductor NCs with a wide range of formulations and composition. This flexibility provides for several opportunities to manipulate and control various properties of these materials. Spectral tunability is among the most distinctive characteristics of colloidal semiconductor NCs. While a straightforward variation in particle size is sufficient to achieve the spectral tunability, colloidal chemistry offers several other unused methods to regulate different material properties as well.

Doping is one of those methods where impurities are used to introduce significant new physical properties into the host. The incorporation of small amount transition metal ions into NCs can achieve the freedom of controlling their various functionalities, and give rise to peculiar properties. For example, this can produce new emission bands at intra-gap energies as well as lead to different magnetic behaviours.

An impurity in a host lattice could be achieved by inserting ions of transition metals with a variable valence as substitutional or interstitial defects (Figure 4). In some particulars, the impurities introduce an atomic like state within the host band gap of the host semiconductor that can have an exchange interaction with valence and conduction bands.

Copper is a well-studied substitutional impurity in II-VI NCs [39-41]. When doped into II-VI NCs such as ZnSe and CdSe, Copper has been shown to exist in a +2 oxidation state [42]. Somewhat surprisingly,  $\text{Cu}^{+2}$  ions substituted into a II-VI lattice do not give rise to any detectable electron paramagnetic resonance (EPR)

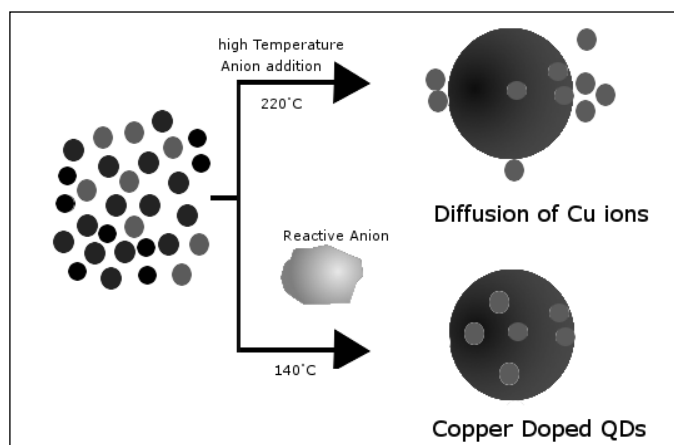


Fig. 4: Schematic of synthesis of Cu doped NCs. Top panel depicts the high temperature synthesis of Cu doped NCs, at high temperature Cu ions diffuse out from the NCs. Bottom panel depicts synthesis of Cu Doped NCs, where reactive anion

signature. This effect has been shown to occur due to line broadening induced by spin-orbit coupling and Jahn-Teller distortions at the tetrahedrally coordinated  $\text{Cu}^{+2}$  center [43]. However the +2 oxidation state of the copper center has been independently confirmed by several other magnetic studies. Most notably, copper ions have been shown to exhibit exchange with semiconductor host, causing the emergence of diluted magnetic semiconducting character in doped NCs. When introduced into a II-VI lattice,  $\text{Cu}^{+2}$  ions give rise to a characteristic, broad emission band [44-45]. The black arrow represents the band edge emission, while the red arrow corresponds to the copper band. Copper emission arises from the radiative decay of a conduction band electron into the copper  $d^9$  level. From this level, the electron is believed to relax nonradiatively into the valence band hole. This process is essentially the same as shown in the process shown in Figure 5.

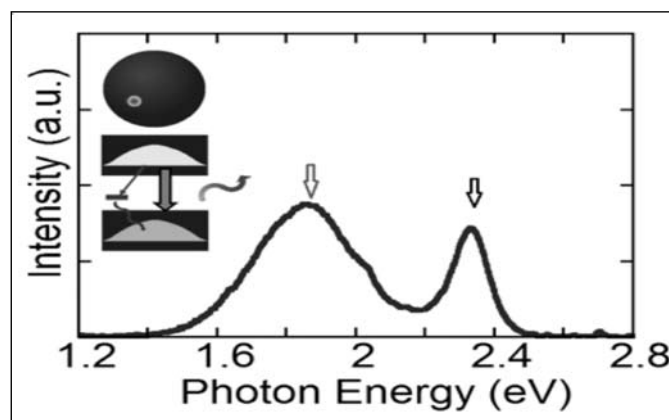


Fig. 5: Absorption and emission spectra of a 1% doped Cu doped CdZnSe QD. Inset, schematic of a copper containing NCs have two alternate pathways for radiative exciton recombination; either direct recombination with a band edge hole or else through the copper center.

Existing syntheses of copper containing NCs give rise only to lightly doped materials containing no more than a percent of the impurity. In contrast, copper-II-VI alloys have been extremely challenging. In particular, any attempt to enhance the doping level beyond a few dopants per NC causes the independent nucleation and precipitation of copper chalcogenides. This is related to the mismatch in reactivities of the cationic precursors. Significantly faster reaction of the copper chalcogenides relative to the other cations can trigger independent nucleation events for the two different chalcogenides. An improved approach is therefore to compensate for the differential reactivities of the cations by employing a very active anion precursor. In this scenario, the NC formation process becomes limited by the rate of diffusion of the two cation precursors rather than their reactivities. To this end, highly reactive acetates of copper, cadmium and zinc were used as the cation precursors. Sodium hydrogen selenide was used as the anion precursor.

It has further been noted that  $\text{Cu}^{+2}$  inclusion proceeds more easily in a CdSe or CdS lattice than in a ZnSe or ZnS lattice. Attempts to increase the concentrations of copper beyond a few percent however disturb the reaction significantly, making precise control over stoichiometry impossible. To improve reliability of the synthesis, CdCuZnSe alloys were adopted, where copper may be conceptually considered to be a replacement for Cd in the lattice. The choice of this composition significantly improved the predictability of the reaction products.<sup>[38]</sup>

The use of a highly reactive anion precursor further complicates the separation of the nucleation and growth steps. In addition, the high temperature required for any ripening mechanism causes simultaneous diffusion of copper ions out of the NC. In this situation, the large activity of the anion precursor itself must be adopted to control growth rates. This occurs in this reaction scheme because of the rapid supersaturation of the initial solution. Post nucleation, the precursors may either be driven to create additional nuclei, or else deposit on existing centers. The choice of a low reaction temperature is critical in this regard since post nucleation, the reactions become diffusion limited, and the greater reaction cross sections for deposition thus preferentially force growth rather than nucleation to become the primary outcome. While this method prevents additional nucleation, it is also evident that this scheme would lead to very rapid size divergence in any growing ensemble. This is avoided by ensuring that the reaction times are very short, and growth itself is a very short term event. The process thus allows the creation of NCs in the concentrated regime [38].

## Controlling morphology by nucleation and growth in templates [46]

Noble metal nanoparticles (MNPs) intensely couple with electromagnetic radiation (UV-Visible) through the excitation of surface plasmon resonance (SPR). SPR are the coherent collective oscillations of the conduction electrons which occur at the interface between metals and dielectrics [47]. Gold and silver shows localised surface plasmon resonance at 530 nm and 400 nm respectively. SPR results in the enhancement of electric field intensity at the surface of the metal nanoparticles (MNPs). This property of SPR has been particularly useful in surface enhanced Raman spectroscopy, sensing and nano-electronics [48-49].

The optical properties or SPR of MNPs is shape and size dependent. The resonance wavelength can be tuned at any desired wavelength from visible to infrared by varying the shape of the metal nanoparticles [50-51]. For instance, gold nanorods show two Plasmon mode viz. transverse mode which corresponds to the oscillations of the electrons perpendicular to the major axis of the rod and longitudinal mode corresponding to the oscillation of the electrons along the major axis of the rod. This longitudinal resonance is tunable from visible to infrared wavelength. Therefore it is an utmost important to control the shape of the metal nanoparticles for a desired application. However Au and Ag possess FCC (face-centred cubic) structure which is highly symmetric leading to difficulties in the synthesis of anisotropic MNPs. The simple reduction of metal salt with reducing agent leads to the formation of spherical particles so as to minimize the surface energy.

The synthesis of anisotropic metallic structures has been performed following different synthetic routes. For example Halder *et. al.* [52] have synthesised the ultrathin Au nanowires through directed attachment of small Au NCs in toluene. On the other method, Phillip *et. al.* have used cetrimonium bromide (CTAB) and silver ion attachment method to synthesised Au bi-pyramidal NCs [53]. Out of these synthetic routes, the template method is facile and simple method for the synthesis of anisotropic metal nanoparticles. In template method, a material of choice is deposited on the substrate. The substrate is generally chosen to be soft which acts as a sacrificial one. Xia and co-worker used galvanic replacement method for the synthesis of hollow Au nanoparticles [54]. Their method involved pre-synthesize of silver nanoparticles and reduction of Au salt like  $\text{HAuCl}_4$  to  $\text{Au}^0$  on the surface of silver nanoparticles. The reduction potential of  $\text{AuCl}_4^-/\text{Au}$  is higher than that of  $\text{Ag}^+/\text{Ag}$ , thus allowing the reduction of  $\text{Au}^{+3}$  into  $\text{Au}^0$ . The silver nanoparticles go into the solution forming  $\text{Ag}^+$  salt and act as the sacrificial template.

This lead to the formation of hollow Au shells whose size and thus the resonance could be tuned by varying the size of silver nanoparticles. On a similar approach various shaped hollow nanoparticles have been synthesised like Au nanocages [55], Au-Ag nanobox [51], Pd nanotubes [56]. The other method utilises the porous material as a template. For example Anodic Aluminium oxide (AAO) template has been used for the synthesis of Au nanodot, nanowires of different metals like Ag, Au, Pd etc. [56].

Apart from shape, the practical application of plasmonic particle is also dependent on its size. Particles with a size smaller than 10 nm suffer from damping due to electron-surface scattering and particles having size greater or comparable to the wavelength of the light exhibit losses due to phase retardation.

Towards this effort single crystalline silver nanorods, having width of around 20 nm and length of around 80 nm, have been synthesised through a template method. Here emphasis is given on depositing a metal nucleus into a suitable template. First Au nanorods of length 80 nm and a width of 20 nm is synthesised by seed mediated approach [57]. Next, a silica layer (30nm) was deposited on Au Nanorods. It was observed that the growth of silica on Au nanorods had to be done in two steps. First, the growth was done under basic condition which deposited the silica layer rapidly. Second the growth was done in neutral pH. This process is a slow process. The advantage of growing two varieties of silica on Au nanorods lies in the fact that it provides the mechanical strength as well as the control on the growth of nanostructures. After the growth of silica on Au nanorods, the etching of gold nanorods was done with Au (CTAB) complex. The etching was done anisotropically as evident from the successive decrease in longitudinal resonance wavelength of the rod and also in the decreases of its amplitude. Figure 6 shows TEM images of partially etched gold nanorods. The etching was continued till a small particle of Au less than 1 nm was left over. Following this, Ag was grown on the template where the left over

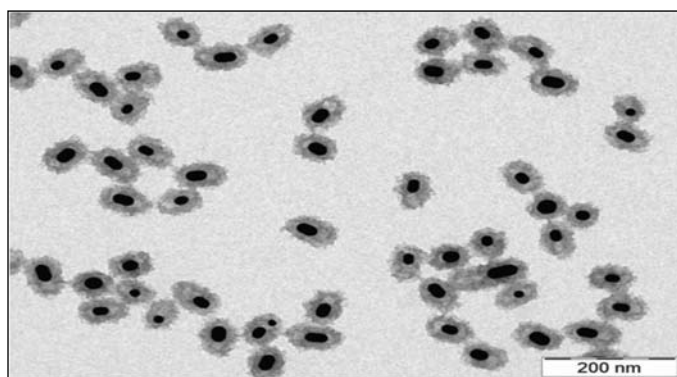


Fig. 6: TEM image of Au nanorods being etched inside a template.

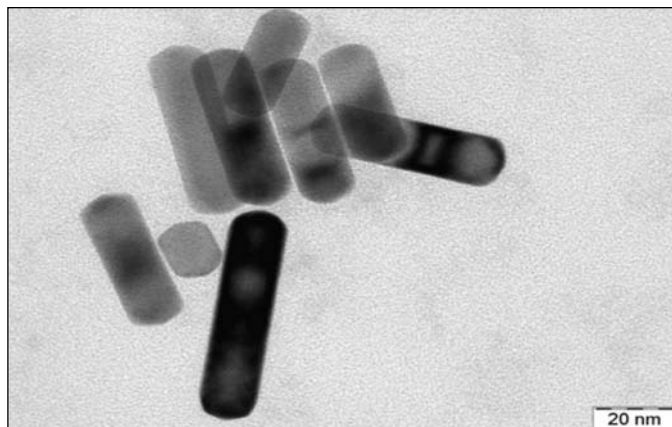


Fig. 7: TEM image of Ag nanorods synthesized via the template nucleation and growth scheme.

small Au act as the nucleating centre. The growth of silver nanorods was confirmed through the evolution of silver surface plasmon resonance [46]. This was tracked through UV-Visible spectra where a red shift of the longitudinal resonance of the silver nanostructure was observed. On the final step the removal of template was done under mild acidic condition in presence of polyvinylpyrrolidone surfactant (PVP). The resultant free silver nanorods are shown in Figure 7. This approach represents a significant departure from the other schemes discussed in this review, in that the concerns of thermodynamic and kinetic control are avoided altogether, rather, shape control is achieved by mechanical regulation afforded by the template [46].

## Conclusion

In conclusion, we have described three different cases of nucleation-growth processes that enable the control of monodispersity, composition and morphology, respectively. These methods are shown to enable the creation of novel nanocrystals as well as to understand the behaviour of existing chemical syntheses.





## Acknowledgement

RM thanks the Council of Scientific and Industrial Research for financial support and IISc for providing facilities. AP thanks the Indian Institute of Science and the Department of Science and Technology for generous funding. AP, RM, BB and DKT thank IISc for providing facilities.

## References:

1. A. J. Nozik, M. C. Beard, J. M. Luther, M. Law, R. J. Ellingson and J. C. Johnson, *Chem. Rev.* **2010**, *110*, 6873-6890.
2. C. R. Kagan, C. B. Murray, M. Nirmal and M. G. Bawendi, *Phys. Rev. Lett.* **1996**, *76*, 1517-1520.
3. Q. Sun, Y. A. Wang, L. S. Li, D. Y. Wang, T. Zhu, J. Xu, C. H. Yang and Y. F. Li, *Nat. Photon.* **2007**, *1*, 717-722.

4. D. V. Talapin, J.-S. Lee, M. V. Kovalenko and E. V. Shevchenko, *Chem. Rev.* **2010**, *110*, 389-458.
5. G. S. Kenath, R. Mahadevu, A. Sharma, V. K. Gangwar, S. Chatterjee, A. Pandey and B. N. Pal, *J. Phys. Chem. C* **2018**, *122*, 3176-3181.
6. R. Mahadevu, A. R. Yelameli, B. Panigrahy and A. Pandey, *ACS Nano* **2013**, *7*, 11055-11063.
7. V. H. Iyer, R. Mahadevu and A. Pandey, *J. Phys. Chem. Lett.* **2016**, *7*, 1244-1248.
8. J. L. West and N. J. Halas, *Annual Review of Biomedical Engineering* **2003**, *5*, 285-292.
9. H. Huang and J.-J. Zhu, *Biosensors and Bioelectronics* **2009**, *25*, 927-930.
10. K. K. Jain, *Clinical Chem.* **2007**, *53*, 2002-2009.
11. R. Mahadevu, H. Kaur and A. Pandey, *Crystengcomm* **2016**, *18*, 759-764.
12. X. G. Peng, J. Wickham and A. P. Alivisatos, *J. Am. Chem. Soc.* **1998**, *120*, 5343-5344.
13. T. Zhang, W. Dong, M. Keeter-Brewer, S. Konar, R. N. Njabon and Z. R. Tian, *J. Am. Chem. Soc.* **2006**, *128*, 10960-10968.
14. E. M. Wong, P. G. Hoertz, C. J. Liang, B.-M. Shi, G. J. Meyer and P. C. Searson, *Langmuir* **2001**, *17*, 8362-8367.
15. N. T. K. Thanh, N. Maclean and S. Mahiddine, *Chem. Rev.* **2014**, *114*, 7610-7630.
16. B. L. V. Prasad, S. I. Stoeva, C. M. Sorensen and K. J. Klabunde, *Chem. Mater.* **2003**, *15*, 935-942.
17. S. Stoeva, K. J. Klabunde, C. M. Sorensen and I. Dragieva, *J. Am. Chem. Soc.* **2002**, *124*, 2305-2311.
18. S. B. Kalidindi and B. R. Jagirdar, *J. Phys. Chem. C* **2008**, *112*, 4042-4048.
19. P. W. Voorhees, *J. Stat. Phys.* **1985**, *38*, 231-252.
20. L. Lindfors, P. Skantze, U. Skantze, M. Rasmusson, A. Zackrisson and U. Olsson, *Langmuir* **2006**, *22*, 906-910.
21. N. G. Bastús, J. Comenge and V. Puntes, *Langmuir* **2011**, *27*, 11098-11105.
22. C. R. Bullen and P. Mulvaney, *Nano Lett.* **2004**, *4*, 2303-2307.
23. R. K. Capek, D. Yanover and E. Lifshitz, *Nanoscale* **2015**, *7*, 5299-5310.
24. M. C. Hanna and A. J. Nozik, *J. Appl. Phys.* **2006**, *100*.
25. A. J. Houtepen, R. Koole, D. Vanmaekelbergh, J. Meeldijk and S. G. Hickey, *J. Am. Chem. Soc.* **2006**, *128*, 6792-6793.
26. B. L. Wehrenberg, C. J. Wang and P. Guyot-Sionnest, *J. Phys. Chem. B* **2002**, *106*, 10634-10640.
27. D. Zhitomirsky, M. Furukawa, J. Tang, P. Stadler, S. Hoogland, O. Voznyy, H. Liu and E. H. Sargent, *Adv. Mater.* **2012**, *24*, 6181-6185.
28. J. Joo, J. M. Pietryga, J. A. McGuire, S. H. Jeon, D. J. Williams, H. L. Wang and V. I. Klimov, *J. Am. Chem. Soc.* **2009**, *131*, 10620-10628.
29. K. L. Hull, J. W. Grebinski, T. H. Kosel and M. Kuno, *Chem. Mater.* **2005**, *17*, 4416-4425.
30. W. K. Bae, J. Joo, L. A. Padilha, J. Won, D. C. Lee, Q. Lin, W.-k. Koh, H. Luo, V. I. Klimov and J. M. Pietryga, *J. Am. Chem. Soc.* **2012**, *134*, 20160-20168.
31. I. C. Baek, S. I. Seok and Y. C. Chung, *Bulletin Korean Chem. Soc.* **2008**, *29*, 1729-1731.
32. J. S. Steckel, B. K. H. Yen, D. C. Oertel and M. G. Bawendi, *J. Am. Chem. Soc.* **2006**, *128*, 13032-13033.
33. S. Boone and O. J. Kleppa, *Thermochimica Acta* **1992**, *197*, 109-121.
34. R. Ganesan, T. Gnanasekaran and R. S. Srinivasa, *J. Nuclear Mater.* **2003**, *320*, 258-264.
35. J. D. Bacha and J. K. Kochi, *Tetrahedron* **1968**, *24*, 2215-2226.
36. S. Gerchakov and H. P. Schultz, *J. Org. Chem.* **1967**, *32*, 1656-1658.
37. I. Moreels, K. Lambert, D. De Muynck, F. Vanhaecke, D. Poelman, J. C. Martins, G. Allan and Z. Hens, *Chem. Mater.* **2007**, *19*, 6101-6106.
38. B. Bhattacharyya, K. Gahlot, R. Viswanatha and A. Pandey, *J. Phys. Chem. Lett.* **2018**, *9*, 635-640.
39. M. Godlewski, W. Lamb and B. Cavenett, *J. Phys. C: Solid State Phys.* **1982**, *15*, 3925.
40. S. Bhaumik, B. Ghosh and A. J. Pal, *Appl. Phys. Lett.* **2011**, *99*, 083106.
41. B. B. Srivastava, S. Jana and N. Pradhan, *J. Am. Chem. Soc.* **2011**, *133*, 1007-1015.
42. R. Viswanatha, S. Brovelli, A. Pandey, S. A. Crooker and V. I. Klimov, *Nano Lett.* **2011**, *11*, 4753-4758.
43. A. Pandey, S. Brovelli, R. Viswanatha, L. Li, J. M. Pietryga, V. I. Klimov and S. A. Crooker, *Nat. Nanotechnol.* **2012**, *7*, 792-797.
44. G. K. Grandhi, R. Tomar and R. Viswanatha, *ACS Nano* **2012**, *6*, 9751-9763.
45. G. K. Grandhi and R. Viswanatha, *J. Phys. Chem. Lett.* **2013**, *4*, 409-415.
46. D. K. Thapa and A. Pandey, *Chemical Physics Letters* **2016**, *658*, 315-318.
47. C. Noguez, *J. Phys. Chem. C* **2007**, *111*, 3806-3819.
48. M. Fleischmann, P. J. Hendra and A. J. McQuillan, *Chem. Phys. Lett.* **1974**, *26*, 163-166.
49. D. L. Jeanmaire and R. P. Van Duyne, *J. Electroanal. Chem. Interface. Electrochem.* **1977**, *84*, 1-20.
50. M. Liu and P. Guyot-Sionnest, *J. Phys. Chem. B* **2005**, *109*, 22192-22200.
51. X. Lu, L. Au, J. McLellan, Z.-Y. Li, M. Marquez and Y. Xia, *Nano Lett.* **2007**, *7*, 1764-1769.
52. A. Halder and N. Ravishankar, *Adv. Mater.* **2007**, *19*, 1854-1858.
53. W. D. Kim, S. Lee, C. Pak, J. Y. Woo, K. Lee, F. Baum, J. Won and D. C. Lee, *Chem. Commun.* **2014**, *50*, 1719-1721.
54. C. M. Copley and Y. Xia, *Mater. Sci. Eng: R: Rep.* **2010**, *70*, 44-62.
55. M. S. Yavuz, Y. Cheng, J. Chen, C. M. Copley, Q. Zhang, M. Rycenga, J. Xie, C. Kim, K. H. Song, A. G. Schwartz, L. V. Wang and Y. Xia, *Nat. Mater.* **2009**, *8*, 935.
56. H.-W. Liang, S. Liu, J.-Y. Gong, S.-B. Wang, L. Wang and S.-H. Yu, *Adv. Mater.* **2009**, *21*, 1850-1854.
57. B. P. Khanal, A. Pandey, L. Li, Q. Lin, W. K. Bae, H. Luo, V. I. Klimov and J. M. Pietryga, *ACS Nano* **2012**, *6*, 3832-3840.

	<p><b>Rekha Mahadevu</b> obtained her 5 year integrated M.Sc in chemistry from the University of Mysore, Mysore Karnataka in the year 2010. Later, she worked as project assistant at JNCASR (2011), Bangalore under the guidance of Prof. Eswarmoorthy. She obtained her PhD degree under the guidance of Prof. Anshu Pandey in the year 2018 at Solid State and Structural Chemistry Unit, Indian Institute of Science, Bangalore, India. Currently, she is working as research associate under the guidance of Prof. Anshu Pandey. Her research interest is synthesis of semiconductor quantum dots and injection of charge carriers into quantum dots.</p>
	<p><b>Biswajit Bhattacharyya</b> obtained his M.Sc in chemistry in 2012 from Visva-Bharati University. Currently he is a fifth year PhD student under the supervision of Anshu Pandey in Solid state and Structural Chemistry Unit, Indian Institute of Science. His research interest is the photophysics and photochemistry of nontoxic semiconductor nanocrystals.</p>
	<p><b>Devkumar Thapa</b> obtained his Master in Science from University of North Bengal, Siliguri. Currently he is pursuing PhD from Indian Institute of Science, Bangalore. His research interest lies on the synthesis of new variant of metallic nanocrystals for novel applications</p>
	<p><b>Anshu Pandey</b> obtained his Ph. D. Degree in 2009 from the University of Chicago. He has been a faculty member at the Solid State and Structural Unit of IISc since 2012. He is interested in the synthesis and spectroscopy of semiconductor and metal nanocrystals</p>

# Advances in Flexible Thin-Film Transistors and Their Applications

Ashutosh Kumar Tripathi<sup>1</sup>, Ishan Choudhary<sup>2</sup>, Deepak<sup>1,2\*</sup>

<sup>1</sup>National Centre for Flexible Electronics, IIT Kanpur, Kanpur – 208016, India

<sup>2</sup>Department of Material Science, IIT Kanpur, Kanpur – 208016, India

E-mail: saboo@iitk.ac.in

## Abstract

Whereas thin film transistor (TFT) is well known over last twenty years, advent of flexible electronics imposes new requirements and constraints. Therefore, we provide an overview of novel TFT technologies that are being developed for flexible electronics applications. While amorphous silicon (a-Si) and Metal-oxide (MOx) semiconductor based TFT technologies are at the forefront, organic thin-film transistor (OTFT) technology provides unique opportunities owing to low processing temperatures, making them compatible with low-cost flexible polymer substrates. In addition to that, both n- and p-type devices can be realized in OTFTs and hence enabling fast and low power complementary circuits. Furthermore, we discuss other novel technologies such as carbon nanotube (CNT) and 2D semiconductors that are still in exploratory phase but possess the potential to outperform conventional TFT technologies not only for their process compliance with flexible substrates but also in terms device performance.

## Introduction

Flexible electronics is an emerging branch of electronics. As per market projection by IDTechx, total market for printed and flexible electronics is estimated to exceed 70 B USD by 2027. Since thin-film transistors (TFT) are basic building blocks of electronics, flexible electronics necessitates development of flexible TFT technology that can be monolithically integrated on flexible substrates such as polymer films, metal sheets and paper. Flexible TFT technology requires temperature as well as process compatibility between materials used in the TFT stack (dielectrics, metals and semiconductor) and substrate materials (polymer film, metal sheets, paper etc.). Performance of conventional Si based transistors depends strongly on processing temperature. While crystalline-Si transistors can deliver very high performance with charge carrier mobility exceeding  $1000 \text{ cm}^2/\text{Vs}$  [1], they not only require very high processing temperature ( $> 900 \text{ }^\circ\text{C}$ ) but also are limited to a maximum substrate size of 300 mm diameter wafer. On the other hand, low-temperature polycrystalline Silicon (LTPS) TFTs with excimer laser annealing can be fabricated at low temperatures offering charge carrier mobilities in the range of  $100 \text{ cm}^2/\text{V. s}$  [2] and are commonly used as TFT backplanes in high resolution active-matrix organic light emitting diode (AMOLED) displays as well as active-matrix liquid crystal displays (AMLCD) in handheld mobile displays [3]. LTPS TFT process is compatible with high grade and expensive polyimide substrates [4]. Process temperature is further reduced down to below  $380 \text{ }^\circ\text{C}$  in hydrogenated amorphous-Si (a-Si:H) TFT array technology. This results in further degradation in the charge carrier mobility ( $\sim 1$

$\text{cm}^2/\text{V. s}$ ) in these TFTs [5 - 7]. But owing to inexpensive fabrication process and excellent spatial uniformity, a-Si:H remains common TFT array technology for backplanes for flat-panel televisions.

While Si based TFTs remain the workhorse for conventional circuits and TFT array technologies, that are typically fabricated on Si-wafers or glass substrates, flexible electronics demand a robust and reliable TFT process compatible with polymer substrates, e.g. polyimide, PET, PEN etc., used in flexible electronics applications. This imposes limit on maximum process temperature in TFT fabrication. In other words, flexible electronics has been a driving force behind development of several novel low-temperature TFT technologies in last couple of decades. We will discuss current status and outlook of some of such promising TFT technologies in subsequent sections.

## Organic TFTs

Organic thin-film transistors (OTFT) has been a topic of research for last several years for flexible electronics applications. We will focus on Organic semiconductor (OSC) films that are used as semiconductor channel in OTFTs. OSCs films can be formed by vacuum deposition as well as printing/coating techniques at low temperatures, typically below  $120 \text{ }^\circ\text{C}$ . Due to low processing temperature, OTFT fabrication is compatible with wide range of flexible substrates. First OTFTs were fabricated as early as in 1987 by Koezuka et al. based on a p-type TFT with polythiophene as semiconductor channel material. These TFTs were fabricated on n-type silicon wafers with thermal  $\text{SiO}_2$  as gate insulator and exhibited hole field-effect mobility of  $\sim 10^{-6} \text{ cm}^2/\text{V. s}$  [8]. Since then OTFT technology has advanced

significantly and TFTs have been demonstrated on several flexible substrates, e.g. PET [9, 10], PEN [11], paper [12, 13] etc.

Compared to inorganic semiconductors, OSCs used in OTFT fabrication possess several unique advantages in addition to the low processing temperature, such as possibility to formulate solution processable inks [14, 15] that enables low-cost and high throughput fabrication routes by printing [16, 17] and good mechanical reliability under bending strain [18]. Furthermore, OSCs are compatible with a number of polymer gate dielectrics [19-26] that enables fabrication of OTFT based arrays and circuits for various flexible electronics applications such as backplanes for displays [27], flexible circuits [28], and X-ray imagers [16, 29] etc.

OTFTs can be made either p-type or n-type depending on the OSC material used for channel. These materials can be further categorized as polymers or small molecules. *Figure 1* gives an overview of typical p-type or n-type OSCs used in OTFTs [30]. As indicated in *figure 1*, majority of OTFT channel materials are p-type due to two primary reasons: (a) high electron injection barrier for stable electrode materials [31] and (b) electron transport in OSCs is much more prone to charge trapping than hole transport because of high reactivity of conduction electrons in LUMO with common environmental species such oxygen and moisture [32].

Initial work on OTFTs was focused on p-type devices using conjugated polymers, such as P3HT, PTAA etc. as semiconductor channel materials [33 - 35]. Typical field-effect mobilities for conjugated polymer based p-type TFTs are in the range of 0.001 - 0.1 cm<sup>2</sup>/V. s. Charge transport mechanism in conjugated polymers is mainly governed by  $\pi$  -  $\pi$  stacking only. Further increase in mobility requires tight molecular packing as observed in small molecules based crystalline OSCs, such as TIPS-Pentacene, diF-TESADT etc. [36 - 38]. One disadvantage of crystalline OSCs is that charge carrier mobility strongly depends on transport direction [39] making them less suitable for large area flexible electronics applications. Several research groups have reported that blending small molecule OSCs with polymers result in better uniformity [40], enhanced performance [41], and also better control over printing of semiconductor channels in OFETs [42] that is essential for a scalable flexible OTFT technology. Over the years, p-type OTFT technology have significantly advanced and mobilities larger than 40 cm<sup>2</sup>/V. s have been reported for small molecules [43, 44] as well as aligned polymer [45] based OTFTs.

While p-type OSCs advanced to high performance and stable OTFTs, n-type OSC based OTFTs were late entrants. Main research challenge for realization of n-type OTFTs has been lowering the LUMO level of n-type OSCs in order to have stable electron transport as well as making it compatible with environmentally stable contact metals. First n-type OTFTs were demonstrated in late 2000s and were based on small molecules with Naphthalene Tetracarboxylic Diimide (NDI) as base molecule. These devices showed very high electron mobilities up to 7.5 cm<sup>2</sup>/V. s [46] but very poor device stability. Several research groups have worked on improving the stability of n-type OSCs by various molecular engineering techniques such as, introduction of fluorinated side-chains [47], incorporating electron withdrawing groups in the naphthalene core [48], and NDI core expansion by fusion of  $\pi$  conjugated moieties to the core [49]. Stability of n-type OTFTs has been significantly improved by introduction of polymer for n-type OSCs [32, 50]. Detailed overview of molecule design and engineering of n-type OSCs can be found in good review articles [30, 51].

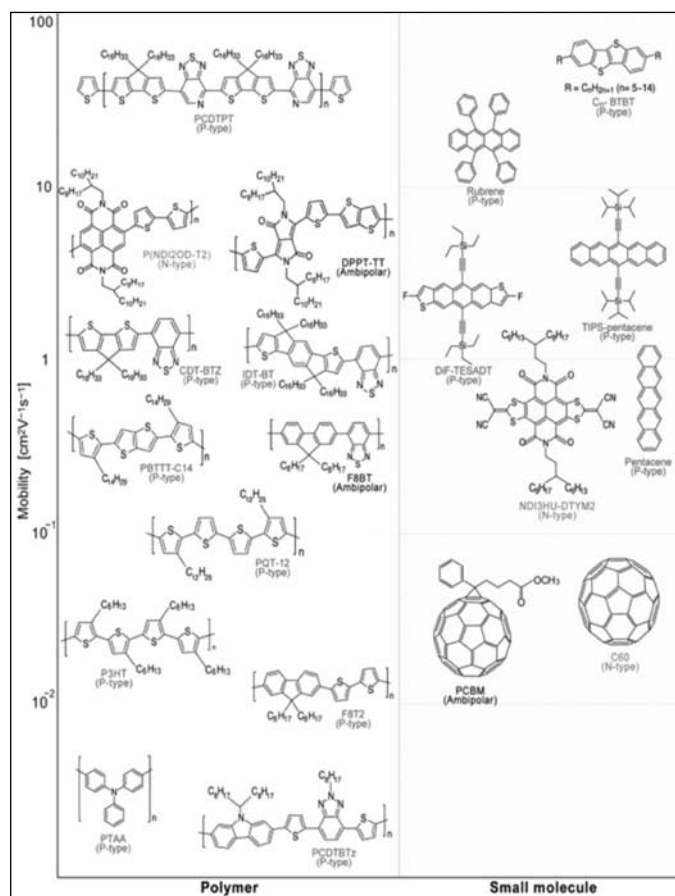


*Fig. 1: Summary of OSC channel materials categorized as polymers and small molecules for n-type and p-type TFTs [30]. (Copyright @ IEEE 2015)*



## Metal Oxide TFTs

Amongst all other “new” TFT technologies, Metal-oxide (MOx) semiconductor based TFTs are found to be most suitable for flexible electronics applications. In case of silicon, the Si atomic orbitals undergo  $sp^3$  hybridization, due to which the band gap is formed as a consequence of splitting of energy into anti-bonding ( $sp^3 \sigma^*$ ) and bonding ( $sp^3 \sigma$ ) energy levels, which are then regarded as conduction band minima (CBM) and valence band maxima (VBM) respectively. However, in case of metal oxide semiconductors, strong ionicity of different ionic species leads to the formation of CBM and VBM. In metal oxides initially, as metal and oxygen atoms are brought closer to each other, charge transfer between them sets the Madelung potential, which stabilizes the material in ionized states. As a consequence, the energy level of oxygen ions (as opposed to the atom) is lowered and that of cation lifted, explaining formation of conduction band due to metal s - orbital and valence band due to p-orbital of oxygen. In MOx semiconductors the CBM is mainly composed of spatially spread spherical “ns” atomic orbitals of metal cations while VBM is made up of “2p” atomic orbitals of oxygen ions ( $O^{2-}$ ). Because of non-directional nature of “ns” orbitals, even Amorphous MOx Semiconductor (AOS) based TFTs can exhibit good performance as opposed to silicon based transistors, where electronic properties depend strongly on the crystallinity of the channel material due to directional nature of  $sp^3$  orbitals [52-54]. MOx semiconductors can be deposited either by vacuum process or by solution processing. Most MOx semiconductors show n-type behavior. However, p-type MOx TFTs are also being investigated.

### 3.1 Vacuum processed n-type MOx TFTs

History of MOx TFTs date back to 1964 when Klasens and Koelmans demonstrated TFTs with n-type tin oxide ( $SnO_2$ ) as semiconductor channel material [55]. MOx based TFTs were overshadowed by a-Si:H TFTs for next few decades until 1996 when  $SnO_2$  [56] and  $In_2O_3$  [57] were demonstrated as n-type semiconductor materials in ferroelectric TFT devices. Subsequently MOx based TFTs gained broad interest amongst the research community and promising results were demonstrated using ZnO as n-type MOx semiconductor in TFTs. Several reports presented ZnO based TFTs with mobility larger than  $1 \text{ cm}^2/\text{V.s}$  [58 – 60], indicating potential of MOx TFTs to replace a-Si:H TFTs. Along with ZnO, several other MOx semiconductors, such as  $In_2O_3$  and  $SnO_2$ , were investigated [61, 62]. In 2003 Fortunato et al. reported rf-sputtered ZnO TFTs with electron mobility  $\sim 20 \text{ cm}^2/\text{V.s}$  [63].

While binary MOx, such as ZnO,  $SnO_2$ , and  $In_2O_3$ , based TFTs were regularly reported in early 2000, despite of their superior performance these TFTs had shortcomings, mainly : (a) device instability, (b) poor uniformity due to crystalline nature, (c) high process temperatures, thus incompatible with flexible substrates, and (d) non-scalable processes. Important breakthrough in MOx was achieved by Nomura et al. in 2004 when they demonstrated multi-component amorphous Indium-Gallium-Zinc Oxide (a-IGZO) based TFTs fabricated on PET substrate at room temperature [64]. Although in this work IGZO was deposited by pulsed laser deposition (PLD), subsequently several works were reported on multi-component MOx TFTs [65 – 67]. Since the report of first a-IGZO TFTs, tremendous progress has been done in this field and there are several reports on IGZO TFTs with good device stability and mobilities larger than  $50 \text{ cm}^2/\text{V.s}$  have been reported [68 - 70] within a short span of time. IGZO TFTs are now poised to replace a-Si:H TFTs for large area backplane technology within next couple of decades.

### 3.2 Solution processed n-type MOx TFTs

While vacuum based sputtered IGZO TFT technology is well established by now, work is still ongoing for developing a solution processed MOx TFTs. Solution processing of TFTs will enable high throughput and low-cost fabrication of flexible electronics circuits using well established printing techniques. Solution processed MOx films can be deposited by two commonly known techniques: (a) nano-particles based inks and (b) metal – salt based sol-gel chemistry. For high performance solution processed TFTs, sol-gel route would be preferred as it offers smoother films and better dielectric-semiconductor interface as compared to nano-particles based route. In 2014 Street et al. demonstrated high performance indium-zinc-oxide (IZO) and IGZO TFTs with mobilities as high as 30 and  $20 \text{ cm}^2/\text{V.s}$  respectively [71]. However, solution processed MOx TFTs require high annealing temperatures ( $> 400 \text{ }^\circ\text{C}$ ) in order to achieve good performance through densification of the semiconductor channel [72]. In order to reduce the TFT process temperature several novel approaches have been demonstrated in last few years. New approaches are mainly based on precursor engineering in combination with modified post-anneal treatments.

In 2008 Meyers et al. demonstrated ZnO TFTs fabricated at  $150 \text{ }^\circ\text{C}$  from aqueous ZnO-precursor yielding a mobility of  $1.8 \text{ cm}^2/\text{V.s}$  [73]. In 2013 Lin et al. established improved performance of ZnO TFTs fabricated through similar route, resulting in TFT mobility of  $\sim 10 \text{ cm}^2/\text{V.s}$  [74]. Maximum process temperature for these TFTs was  $180 \text{ }^\circ\text{C}$ . TFTs with other MOx semiconductors fabricated

through aqueous precursor route have been reported [75, 76]. In 2010 Banger et al. demonstrated IZO TFTs fabricated at 230 °C through metal alkoxide based precursors [77]. These TFTs showed mobility of 7 cm<sup>2</sup>/V.s and good device stability under gate bias. Another approach towards low temperature solution processed MOx TFTs is to utilize combustion chemistry. In this approach the precursor solution consists of a fuel source that oxidizes metal compound into MOx. Self-heating reaction in the precursor films assists in lowering thermal annealing temperature. In 2011 Kim et al. demonstrated several MOx TFTs via combustion processing [78]. In<sub>2</sub>O<sub>3</sub> TFTs fabricated with this process had maximum processing temperature of 200 °C and exhibited mobility ~ 6 cm<sup>2</sup>/V.s on solution processed Al<sub>2</sub>O<sub>3</sub> gate dielectric. Further modifications in precursor chemistry for improved TFT performance has been reported by several groups [79-81]. In 2015 Rim et al. reported In<sub>2</sub>O<sub>3</sub> TFTs fabricated from aqueous nitrate ligand-based indium precursor at maximum processing temperature of 250 °C exhibiting mobility larger than 36 cm<sup>2</sup>/V.s [76]. Further improvement in TFT performance was achieved by bilayer heterojunction MOx TFTs. Faber et al. reported bilayer ZnO/In<sub>2</sub>O<sub>3</sub> heterojunction TFTs processed through aqueous precursor route resulting in mobility ~ 45 cm<sup>2</sup>/V.s [82]. In addition to precursor engineering, innovative post fabrication treatments such as annealing in O<sub>2</sub>/O<sub>3</sub> rich environment [83], high pressure annealing [84], microwave annealing [85], and TFT channel activation by deep ultra-violet exposure [86] have been suggested to achieve high performance MOx TFTs.

### Exploratory technologies for high performance flexible TFTs

As discussed in previous sections, during last few decades several new TFT technologies have been developed for flexible electronics applications. However, all new technologies have one or more of following issues: (a) Poor device stability (OTFTs), (b) Lack of complementary (both n- and p-type MOx) TFT processes, and (c) Low TFT switching speed compared to LTPS or Si MOSFET (OTFTs and MOx TFTs). Above have been key drivers for further development of novel TFT technologies. In this section we will briefly touch upon some of them.

#### 4.1 Carbon nanotube TFTs

Carbon nanotubes (CNTs) is seen as a promising semiconductor channel material for its exemplary electronic, optical as well as mechanical properties [87, 88]. CNTs are one-dimensional materials that can be conceptualized as being formed by rolling of a graphene sheet [89]. CNTs have been demonstrated as p-type channel material for solution processed TFTs. Mobilities in the range of few

10s of cm<sup>2</sup>/V.s have been typically reported for CNT based p-type TFTs [90-92]. For aligned single wall CNTs, mobilities as high as 3500 cm<sup>2</sup>/V. s have been reported [93]. High performance of CNT based TFTs make them a potential candidate for p-type TFTs in a flexible CMOS logic in combination with metal-oxide based n-type TFTs [94]. Though key challenges in CNT remains as material synthesis as well as post growth/synthesis separation of metallic and semiconducting CNTs [87].

#### 4.2 2D semiconductor TFTs

Flexible electronics demand materials that exhibit excellent optoelectronic as well as mechanical properties. Two-dimensional materials such as graphene, transition metal dichalcogenides (TMD), transition metal carbides and several other type of materials have been studied for future electronics applications [95, 96]. Out of many, graphene is considered to be the most promising 2D electronic material [97]. Graphene sheets are composed of honeycomb-like network of covalently bonded carbon atoms. Graphene is a zero band-gap material and in order to use it as a TFT channel material, band opening is required. Band opening is achieved by formation of Graphene nano-ribbons [98]. It has been demonstrated that current drive capacity of graphene TFTs increases with decreasing width of the nano-ribbons [99]. Wang et al. have demonstrated graphene TFTs, with nano-ribbons of 10 nm width, exhibiting an ON/OFF ratio > 10<sup>6</sup> and mobility ~ 200 cm<sup>2</sup>/V. s [98]. Fabrication of nano-ribbon is a challenging process and it has been figured out that graphene-inorganic heterojunction can also open-up the band-gap in graphene nano-sheet [100]. For example, Roy et al. have demonstrated Graphene/BN/MoS<sub>2</sub> based vertical TFTs with ON/OFF ratio > 10<sup>6</sup> and electron mobility ~ 33 cm<sup>2</sup>/V. s [101]. In addition to graphene, TMDs such as MoS<sub>2</sub>, WS<sub>2</sub>, MoSe<sub>2</sub>, and WSe<sub>2</sub> have also been of interest for high performance flexible n-type TFT channel materials.

#### 4.3 p-type MOx TFTs

As discussed in *sections 3*, good electron transport is favourable in MOx semiconductors because their CBM is characterized by overlap of spherical “ns” orbitals of transition metal ions. However, VBM in MOx semiconductors is typically characterized by localized “2p” orbitals of oxygen, causing poor hole mobility in these materials. Due to the limitations imposed by electronic structure, only very few MOx have been found suitable for p-type TFTs. Cu<sub>x</sub>O and SnO<sub>x</sub> are widely investigated p-type MOx semiconductors. In case of SnO<sub>x</sub>, VBM is formed by hybridization of oxygen (2p) and Sn (5s) orbitals providing electronic structure favourable for hole

transport [102]. First p-type  $\text{SnO}_x$  TFTs required very high process temperatures even for low performance devices [103]. Advances in material science and various process optimizations enabled several research groups to achieve  $\text{SnO}_x$  based p-type TFTs nowadays with hole mobility ranging between 1 – 10  $\text{cm}^2/\text{V.s}$  [104 – 106]. In case of  $\text{Cu}_x\text{O}$ , VBM is formed by hybridization of oxygen (2p) and Cu (4d) orbitals [107].  $\text{Cu}_x\text{O}$  based p-type TFTs have been reported with mobility up to 4.3  $\text{cm}^2/\text{V.s}$  [108]. Several other p-type  $\text{MO}_x$  TFTs, such as NiO [109], doped ZnO nanowire [110], Zn doped  $\text{Ga}_2\text{O}_3$  [111] etc. have been reported but very few results are available on flexible substrates [112-114] due to relatively high processing temperatures and poor stability of these devices.

### Applications and outlook for flexible TFTs

In previous sections we have given an overview of potential TFT technologies for flexible electronics applications. It is evident that  $\text{MO}_x$  based n-type TFTs are in most advanced stage followed by OTFTs and other technologies. In **Table 1** we provide a brief summary of few flexible electronics applications that have been realized using above mentioned TFT array technologies.

**Table 1 Summary of TFT types and their deployment in some flexible electronics applications. (VP stands for vacuum processed, SP stands for solution processed)**

Technology	Flexible Electronics Applications
<b>MO<sub>x</sub> TFTs</b>	
n-type (VP)	Display backplanes [115-118], circuits/RFID [119 - 122], imager [123]
n-type (SP)	Display backplanes [124, 125], circuits [126]
Complementary	Fully $\text{MO}_x$ complimentary circuits [127, 128], hybrid Organic/ $\text{MO}_x$ circuits [129,130]
<b>OTFTs</b>	
p-type (VP & SP)	Display backplanes [27, 131, 132], circuits [28, 133], imager [16, 29]
n-type (VP & SP)	Display backplanes [134]
Complementary	Circuits [135, 136]
<b>Other technologies</b>	
CNT	Logic circuits [137]
2D semiconductor	Graphene based electronics [138], TMD based sensors [95,139,140]

Above are only a few examples of applications of new TFT technologies in flexible electronics. While  $\text{MO}_x$  based n-type TFT array technology is already in

advance stages, OTFT technology offers complementary circuits due to availability of both n- and p-type OSCs that can be processed at low temperatures. CNT and 2D semiconductor based TFT technologies have potential to offer ultimate device performance including mechanical robustness for ultra-thin and compliant flexible electronics but more work needs to be done towards an optimal and scalable process.

### References:

1. "Electrical, Electronics, and Digital Hardware Essentials for Scientists and Engineers", By Ed Lipinsky, DOI:10.1002/9781118414552, 2013
2. T. Sameshima et al., *IEEE Electron Device Lett.*, **1986**, 7, 276.
3. N. Nodera et al., *Journal of the SID* 24/6, (2016).
4. X. Gao et al., *J. Disp. Technol.*, **2015**, 11, No. 8.
5. F. Morin, *Microelectronic Engineering* **1992**, 19, 171.
6. A. Nathan et al., PROC. 22nd Intl. Conference on Microelectronics (MIEL 2000), **1**, NIS, SERBIA, 14-17 MAY, (2000).
7. H. Gleskova et al., *IEEE Electron Device Lett.*, **1999**, 20, No. 9, 473.
8. H. Koezuka et al., *Synthetic Metals*, **1987**, 18, 699-704.
9. W. Xu et al., *Sci. Rep.*, **2016**, 6, pp 29055.
10. J. Jang, *Material Today*, **2006**, 9, 4.
11. K. Fukuda et al., *Sci. Rep.*, **2014**, 4, pp 3947.
12. Y.-H. Kim et al., *Electron Device Lett.*, **2004**, 25, No. 10.
13. A. T. Zocco et al., *Nanotechnology*, **2014**, 25, 094005.
14. S. K. Park et al., *IEEE Electron Device Lett.*, 2007, 28, No. 10.
15. D. J. Gundlach et al., *Nature Materials*, **2008**, 7, 216.
16. L. Zhang et al., *Sci. Rep.*, **2013**, 3, pp 1080.
17. S. Park et al., *PNAS*, **2015**, 112, 18, 5561–5566.
18. M. Kaltenbrunner et al., *Nature*, **2013**, 499, 458.
19. J. Veres et al., *Adv. Funct. Mater.*, **2003**, 13, 3, pp. 199–204.
20. W. Huang et al., *Nanos. Res. Lett.*, **2014**, 9, pp. 1–8.
21. L.-L. Chua et al., *Nature*, **2005**, 434, pp. 194–199.
22. S. Pyo et al., *Appl. Phys. Lett.*, **2005**, 86, p. 133508.
23. L. Feng et al., *Sci. Rep.*, **2016**, 6, p. 20671.
24. W. Tang et al., *Adv. Electron. Mater.*, **2016**, 5, p. 1500454.
25. H. Sirringhaus et al., *Science*, **2000**, 290, pp. 2123–2126.
26. L. Feng et al., *IEEE Electron Device Lett.*, **2013**, 34, pp. 129–131.
27. M. Katsuhara et al., *Journal of the SID* **2010** 18/6.
28. K. Myny et al., *IEEE J. Solid-State Circuits*, **2012**, 47, 1.
29. A. Kumar et al., *Proc. SPIE 9137*, Organic Photonics VI, **2014**, 91370Q.
30. X. Guo et al., *IEEE Trans. Electron Devices*, **2017**, 64, 5.
31. C. D. Dimitrakopoulos et al., *Adv. Mater.*, **2002**, 14,.
32. H. Yan et al., *Nature*, **2009**, 457, 679–686.
33. J.-F. Chang et al., *Chem. Mater.*, **2004**, 16, pp. 4772–4776.
34. J. Veres et al., *Adv. Funct. Mater.*, **2003**, 13, pp. 199–204.

35. I. McCulloch et al., *Nature Mater.*, **2006**, 5, pp. 328–333.
36. S. K. Park et al., *Appl. Phys. Lett.*, **2007**, 91, p. 063514.
37. S. K. Park et al., *Appl. Phys. Lett.*, **2008**, 93, p. 043301.
38. T. Sakanoue et al., *Nature Mater.*, **2010**, 9, pp. 736–740.
39. M. E. Gershenson et al., *Rev. Mod. Phys.*, **2006**, 78, 973.
40. J. Smith et al., *Adv. Mater.*, **2012**, 24, pp. 2441–2446.
41. K. L. McCall et al., *Adv. Funct. Mater.*, **2014**, 24, pp. 3067–3074.
42. B. K. C. Kjellander et al., *Adv. Mater.*, **2010**, 22, 4612–4616.
43. J. Liu et al., *Nat. Commun.*, **2015**, 6, 10032.
44. Y. Yuan et al., *Nat. Commun.*, **2014**, 5, 3005.
45. C. Luo et al., *Nano Lett.*, **2014**, 14, 2764–2771.
46. D. Shukla et al., *Chem. Mater.*, **2008**, 20, 7486–7491.
47. H. E. Katz et al., *Nature*, **2000**, 404, 478–481.
48. W. Hong et al., *Chem. Commun.*, **2012**, 48, 8413.
49. X. Gao et al., *J. Am. Chem. Soc.*, **2010**, 132, 3697–3699.
50. F. S. Kim et al., *Adv. Mater.*, **2010**, 22, 478–482.
51. J. T. E. Quinn et al., *J. Mater. Chem. C*, **2017**, 5, 8654–8681.
52. E. Fortunato et al., *Adv. Mater.*, **2012**, 24, 2945–2986.
53. L. Petti et al., *App. Phys. Rev.*, **2016**, 3, 021303.
54. T. Kamiya et al., *Sci. Technol. Adv. Mater.*, **2010**, 11, 044305.
55. H. A. Klasens et al., *Solid-State Electron.*, **1964**, 7, 701.
56. M. W. J. Prins et al., *Appl. Phys. Lett.*, **1996**, 68, 3650.
57. C. H. Seager et al., *Appl. Phys. Lett.*, **1996**, 68, 2660.
58. R. L. Hoffman et al., *Appl. Phys. Lett.*, **2003**, 82, 733.
59. P. F. Carcia et al., *Appl. Phys. Lett.*, **2003**, 82, 1117.
60. E. M. C. Fortunato et al., *Appl. Phys. Lett.*, **2004**, 85, 2541.
61. D. Zhang et al., *Appl. Phys. Lett.*, **2003**, 82, 112.
62. R. E. Presley et al., *J. Phys. D: Appl. Phys.*, **2004**, 37, 2810.
63. E. M. C. Fortunato et al., *Adv. Mater.*, **2005**, 17, 590.
64. K. Nomura et al., *Nature*, **2004**, 432, 488.
65. W. Jackson et al., *Appl. Phys. Lett.*, **2005**, 87, 193503.
66. N. L. Dehuff et al., *J. Appl. Phys.*, **2005**, 97, 64505.
67. J.-S. Park et al., *Appl. Phys. Lett.*, **2007**, 90, 262106.
68. Y. S. Rim et al., *ACS Nano*, **2014**, 8, 9680.
69. S. Hu et al., *IEEE Electron Device Lett.*, **2017**, 38, 7.
70. Kim, S. I. et al., *IEDM Tech. Dig.*, **2008**, 73.
71. R. A. Street et al., *ACS Appl. Mater. Interfaces*, **2014**, 6, 4428–4437.
72. S. Park et al., *Mater. Sci. and Engg.: R: Reports*, **2017**, 114, 1–22.
73. S. T. Meyers et al., *J. Am. Chem. Soc.*, **2008**, 130, 17603–17609.
74. Y. H. Lin et al., *Adv. Mater.*, **2013**, 25, 4340–4346.
75. Y. Hwan Hwang et al., *NPG Asia Materials*, **2013**, 5, e45.
76. Y. S. Rim et al., *Chem. Mater.*, **2015**, 27, 5808–5812.
77. K. K. Banger et al., *Nat. Mater.*, **2011**, 10, 45–50.
78. M. G. Kim et al., *Nat. Mater.*, **2011**, 10, 382–388.
79. J. W. Henneke et al., *J. Am. Chem. Soc.*, **2012**, 134, 9593–9596.
80. Y. H. Kang et al., *J. Mater. Chem. C*, **2014**, 2, 4247–4256.
81. B. Wang et al., *Adv. Electron. Mater.*, **2016**, 2, 1500427.
82. H. Faber et al., *Sci. Adv.*, **2017**, 3, e1602640.
83. S. Y. Han et al., *J. Am. Chem. Soc.*, **2011**, 133, 5166–5169.
84. Y. S. Rim et al., *J. Mater. Chem.*, **2012**, 22, 12491.
85. T. Jun et al., *J. Mater. Chem.*, **2011**, 21, 1102–1108.
86. Y. H. Kim et al., *Nature*, **2012**, 489, 128–132.
87. Y. Wu et al., *J. Nanomaterials*, **2013**, 2013, 627215.
88. D.-M. Sun et al., *Small*, **2013**, 9, No. 8, 1188–1205.
89. S. Iijima, *Nature*, **1991**, 354, 6348, pp. 56–58.
90. C. Wang et al., *Nano Letters*, **2009**, 9, 4285–4291.
91. D.-M. Sun et al., *Nat. Nanotech.*, **2011**, 6, 156–161.
92. C. Wang et al., *ACS Nano*, **2010**, 4, 12, 7123–7132.
93. F. N. Ishikawa et al., *ACS Nano*, **2009**, 3, 1, 73–79.
94. W. Honda et al., *Sci. Rep.*, **2015**, 5, 15099.
95. W. Choi et al., *Materials Today*, **2017**, 20, 3.
96. Z. Zhu et al., *RSC Adv.*, **2017**, 7, 17387.
97. K. S. Novoselov et al., *Science*, **2004**, 306, 666–669.
98. X. Li et al., *Science*, **2008**, 319, 1229–1232.
99. X. Wang et al., *Phys. Rev. Lett.*, **2008**, 100, 1586–1594.
100. C. R. Dean et al., *Nat. Nanotechnol.*, **2010**, 5, 722–726.
101. T. Roy et al., *ACS Nano*, **2014**, 8, 6259–6264.
102. Y. Ogo et al., *Phys. Status Solidi A*, **2009**, 206, 2187.
103. Y. Ogo et al., *Appl. Phys. Lett.*, **2008**, 93, 032113.
104. J. A. Caraveo-Frescas et al., *Sci. Rep.*, **2014**, 4, 5243.
105. Y.-J. Han et al., *IEEE Electron Device Lett.*, **2014**, 35, 1260.
106. P. C. Hsu et al., *Jpn. J. Appl. Phys., Part 1*, **2013**, 52, 05DC07.
107. E. Fortunato et al., *Appl. Phys. Lett.*, **2010**, 96, 192102.
108. X. Zou et al., *IEEE Electron Device Lett.*, **2010**, 31, 827.
109. Y. Chen et al., *Thin Solid Films*, **2015**, 592, 195.
110. G. D. Yuan et al., *Nano Lett.*, **2008**, 8, 2591.
111. P. C. Chang et al., *Appl. Phys. Lett.*, **2005**, 87, 222102.
112. R. F. P. Martins et al., *Adv. Funct. Mater.*, **2013**, 23, 2153.
113. J. A. Caraveo-Frescas et al., *Sci. Rep.*, **2014**, 4, 5243.
114. A. Dindar et al., *Appl. Phys. Lett.*, **2011**, 99, 172104.
115. M. Nag et al., *J. Soc. Inf. Disp.*, **2013**, 21, 129.
116. T. Yamamoto et al., *IEEE Trans. Ind. Appl.*, **2012**, 48, 1662.
117. Y. Nakajima et al., *J. Soc. Inf. Disp.*, **2014**, 22, 137.
118. A. Chida et al., in *SID Symp. Dig. Tech. Pap.*, **2013**, pp. 196–198.
119. A. K. Tripathi et al., *IEEE Trans. Electron Devices*, **2015**, 62, 4063.
120. C. Zysset et al., *Electron. Lett.*, **2011**, 47, 691.
121. K. Myny et al., in *IEEE Int. Solid-State Circuits Conf. (ISSCC)*, **2015**, pp. 294–296.
122. B.-D. Yang et al., *ETRI Journal*, **2013**, 35, Number 4.
123. A. V Bremen, in *Flextech 2017*, June 19 – 21, Monterey, California, USA (2017)
124. S. J. Heo et al., *J. Information Disp.*, **2013**, 14, 79–87.
125. B. Cobb et al., *SID 2014 DIGEST*, **2014**, 45, pp 161–163.

126. A. Bashir et al., *Adv. Mater.*, **2009**, 21, 2226-2231.  
 127. R. Martins et al., *Adv. Mater.*, **2011**, 23, 4491.  
 128. A. Dindar et al., *Appl. Phys. Lett.*, **2011**, 99, 172104.  
 129. D. I. Kim et al., *Org. Electron.*, **2012**, 13, 2401.  
 130. K. Nomura et al., *Appl. Phys. Lett.*, **2010**, 96, 263509.  
 131. K. Suzuki et al., *International Symposium on Electronics Paper* **2010**.  
 132. G. S. Ryu et al., *Org. Electron.*, **2013**, 14, 1218-1224.  
 133. A. Sou et al., *Org. Electron.*, **2014**, 15, 3111-3119.  
 134. W.-C. Tang et al., *SID 2015 Digest*, **2015**, 46, 973 -975.  
 135. T. N. Ng et al. , *Sci. Rep.*, **2015**, 5, 13457.  
 136. W. T. T. Smaal et al., *Org. Electron.*, **2012**, 13, 9, 1686-1692.  
 137. D. Lee et al., *Sci. Rep.*, **2016**, 6, 26121.  
 138. H. Jang et al., *Adv. Mater.*, **2016**, 28, 4184-4202.  
 139. D.J. Late, et al. *ACS Nano*, **2013**, 7, 4879.  
 140. K. K-zadeh, et al. *ACS Sens.*, **2016**, 1, 5.



**Dr. Ashutosh Tripathi** did his M.Sc. from IIT Kanpur and received PhD degree in physics from University of Stuttgart, Germany in 2008. After that he started working at Holst Centre, Netherlands as a senior researcher where he was involved in development of TFT backplane technology for various flexible electronics applications. Since 2015 he has been an R&D Team Leader at National Centre for Flexible Electronics at IIT Kanpur. He has broad research interests in the field of TFT based flexible and wearable electronics.



**Dr. Ishan Choudhary** has defended his thesis in 2018 titled "Flexible substrate compatible solution processed indium-gallium-zinc-oxide based transistors and its P-N heterojunction diodes with copper oxide" at Indian Institute of Technology Kanpur (IITK), Kanpur. His current research interest is in metal oxide based transistors and heterojunction diodes.



**Professor Deepak** obtained his B. Tech. degree from the IIT Kanpur, M. S. from University of Florida, Gainesville, Florida (USA) and Ph. D. from University of California, Berkeley, California (USA). After a year-long post-doctoral work at the Argonne National Laboratory, Illinois (USA) and three years in semiconductor device manufacturing and design at Motorola Inc., Phoenix, Arizona (USA), he joined IIT Kanpur in 1997.

# Conjugated Polymers: New Insights via Continuous Flow Syntheses

Anil Kumar<sup>1\*</sup> and Sreelekha P Gopinathan<sup>2</sup>

<sup>1</sup>Department of Chemistry, National Centre of Excellence in Technologies for Internal Security (NCETIS), National Centre for Photovoltaic Research and Education (NCPRE)

<sup>2</sup>Centre for Research in Nanotechnology and Science  
Email: anilkumar@iitb.ac.in

## Abstract

Conjugated polymers provide a solution to the large-area applications for economically viable low-cost optoelectronic devices. However, the quality and quantity of the conjugated polymers and their reproducibility during the development of any large-scale application remains one of the major challenges. These challenges arise because of the limitations of batch methodologies adopted for syntheses. To overcome the boundaries of traditional batch techniques, a need for additional motivating factors which benefits the synthetic chemists is required. In recent past, continuous flow processes for the production of various materials is gaining interest due to its batch-to-batch reproducibility, easy scale-up, enhanced heat and mass transfer leading to better control over the critical molecular design parameters. Potential to scale-up being the most important advantage to the industry, in addition, to yield, reproducibility, safety, time and automation. This article reviews some of the recent developments in the synthesis of conjugated polymers via continuous flow synthesis.

## Introduction

Organic electronics is a fast growing area of interdisciplinary science that takes advantage of the ease of material fabrication in an environment-friendly way. The fabrication methods for organic devices are simpler and cost-effective. In addition to this, devices made out of organic materials are flexible, lightweight and economical, as opposed to the inorganic semiconducting materials and their devices. Also, inorganic electronics depends strongly on the limited sources of depleting natural resources whereas; wonders of organic electronics involve the low-cost synthesis of the semiconductor materials from renewable resources. In an interesting review, Stephen Forrest classifies organic films or electronic materials in three categories: small molecules, biological molecules, and polymers [1]. Recent studies on organic semiconductors have concentrated more on polymeric materials because of its processability [2,3]. Thin films of organic semiconductors can be prepared on readily available substrates like glass and plastics via printing or coating techniques [4,5]. Commercially, there has been a stimulating growth of organic electronics and the range of products that are engineered include organic light emitting diodes (OLEDs), organic photovoltaic cells (OPVs), organic radio frequency identification tags (RFIDs), super-capacitors, batteries, chemical and biological sensors, and organic thin film transistors (OTFT) among many others [6]. The industry is foreseen to touch around \$80 billion within a decade [7]. Polymeric materials are used for making thin films in the fabrication of LEDs and are used in displays for

televisions, computers and mobile phones. Solution-processed fabrication techniques of polymeric materials has enhanced the organic photovoltaic sector where conjugated polymers are used as active layer to absorb light energy and convert to electrical energy and a power conversion efficiency (PCE) of 13% has achieved recently [8]. RFIDs are now rapidly replacing the traditional barcodes with the steep decrease in the cost of production of organic TFTs. TFTs have also been successfully recognized in the applications of flexible electronic paper, memory devices, and sensors [9]. The charge carrier mobility is an important factor in the efficiency of organic devices and polymer semiconductors have recently achieved a remarkable charge carrier mobility up to  $10 \text{ cm}^2/\text{V-s}$  [10,11].

For the development of any large-area application, both quality (in terms of reproducibility, purity, and control over critical molecular design parameters) [12] and quantity (large volumes for printing) [13] are important. Since most of the traditional synthesis of conjugated polymers relies on batch methods, control over both quality and quantity during scale-up becomes major challenges. Towards this, continuous flow processes provide a potential alternative.

## Continuous Flow Process

Until a decade ago continuous flow synthesis or processing was more prevalent in oil refinery, biotechnological production, and petrochemical industry [14]. However, recently continuous flow processing technology has revolutionized the synthesis strategy of

organic materials and, this has initiated the thoughts in the synthesis of polymers too [15]. This technology has matured from lab technique to several commercially available reactors that have paved the way to the growth of the technology and is widely accepted in research institutions as well as industries [16]. A diverse range of industries like agrochemicals, specialty chemicals, organic dyes, natural products and particularly pharmaceutical industries has adapted to continuous flow synthesis because of its desirable features [17-23]. Many researchers working in the area of flow chemistry has written reviews about benefits as well as challenges in flow chemistry in addition to the possibilities of the technique for organic synthesis [21, 24-32]. Benefits of the continuous flow process include enhanced heat transfer characteristics, effective mass transfer, safety, isolation of air and moisture from the reaction zone, high pressure and high-temperature reaction feasibility. The technology also facilitates rapid experimentation, faster optimization and faster library creation of molecules because of its modular nature. Furthermore reduced waste generation, lesser solvent usage and use of fewer utilities allows the technology to be a major player in green chemistry [26,33,34]. Besides chemical and material synthesis continuous flow synthesis has set foot in chemical biology as well where a fully automated peptide synthesis was carried out by MIT researchers with a total synthesis time of 40 seconds per amino acid residue [35]. Most interestingly a Chinese agrochemical company demonstrated the potential of continuous flow synthesis for low footprint by replacing 20 batch reactors with a 7.5 m length flow reactor [36]. In various countries, continuous flow synthesis/flow chemistry has already been intensively taught in academic curricula [37]. Very recently the potential to address the involvement of flow chemistry in the various stages of chemical education has been reported by Rutjes and coworker [38]. Continuous flow synthesis has paved the way to innovation in science by opening up new pathways in chemistry with integration of engineering and informatics, thereby making end to end automation possible by taking care of chemical transformations, separations, crystallization, drying, and even formulation [39-43]. The team of researchers engaged in flow chemistry are from different disciplines like chemistry, physics, chemical engineering, mechanical engineering, material science, and so on which shows the potential and multidisciplinary aspects of this technology. Improved understanding of the flow chemistry and the processes is enhancing the acceptance of the technology to all fields of science. The immense potential of the technology to synthesize, down-stream process, and analyze in-line, helps to do process intensification of many

existing processes with much ease at a very low cost. Since the levels of reproducibility and consistency of continuous flow processing are much better compared to conventional batch synthesis, the product profiles in material synthesis are also improved [44].

For the growth of the chemical industry, continuous flow synthesis has played an immense role in terms of safety, economy, and quality. Safety regarding handling of hazardous chemicals, chemistries which were considered as forbidden became feasible. Because of the high surface area of reaction environment, rapid heat exchange occurs thereby avoiding runaway reactions and also it can safely handle unstable, reactive intermediates. Boosting reaction rates by working in Novel Process Windows (NPW) is another key advantage of continuous flow synthesis. The economy in terms of automation by integrating multistep process by which less workforce is required and low footprint for setting up the facility. Development of a process takes only minimum time using this technology because the process parameters can be rapidly optimized as well as there are minimum downstream processes. In addition to this, the scale-up of reactions are straightforward with high reproducibility which is the most attractive feature, so far industry is concerned. With superior characteristics and also better yield, flow chemistry has evolved as a potential technology for efficiently synthesizing materials in the last two decades. Because of the above said extremely attractive features, the acceptance of the continuous flow synthesis is enhanced and there is an exponential growth in the number of research publications in continuous flow synthesis and more synthetic processes being optimized particularly in the pharmaceutical research [22,31].

### **Continuous Flow Synthesis of Conjugated Polymers**

In the last two decades, significant efforts are directed towards bringing organic electronics to market by roll to roll printing and inkjet printing of flexible, lightweight, cost-effective devices [4,5,45-49]. For large area applications in organic electronics significant quantity of high-quality material is required as the active layer, conjugated polymers are the most widely used materials in organic electronics, and the quality and quantity of the polymers is very crucial for research as well as commercialization.

High molecular weight, low polydispersity, defect-free, polymers with minimum or no impurities are considered to be the qualities of polymeric material which is used as active layer material in organic electronic devices [50-52]. Also, printing is the principal technique used for preparing organic electronic devices and for optimization of the performance of the devices many trials need to be carried

out, and these trials of printing consume a lot of material. Moreover, when it comes to more quantity, multiple batches need to be prepared, and batch to batch reproducibility also has to be maintained. Synthesizing more quantity of these materials in the batch has safety issues because of inefficient heat transfer under batch conditions and multiple, small batches give materials of different quality which further hinders the research and development in this area. In order to explore the multi-gram production of conjugated polymers with superior quality, continuous flow synthesis would be the best option. A solar park facility showed by Krebs *et al.* supports our observations of the requirement of quantity and quality of the material [13]. Using roll to roll printing technique an OPV array of 90 m<sup>2</sup> area was made by Krebs's group and deployed. Even if we consider 10 g of active material in an array, we would require hundreds of grams of material for optimization and final printing of the devices. Commercially, poly(3-hexylthiophene) (P3HT) and phenyl-C61-butyric acid methyl ester (PC<sub>61</sub>BM) are the only organic electronics materials offered in large quantities, that too batch synthesized. Availability of good quality cutting edge organic electronics material in multi-grams is still a vision; hence flow chemistry is the present best solution for tackling the requirement. There is only less than 20 publications in the field of organic conjugated electronics materials via continuous flow synthesis and shows the nascent stage of the technology in the area of polymer chemistry. In this review, we try to bring to the notice of the scientific community the advantages and possibilities of continuous flow synthesis for organic electronics.

### Continuous Flow Synthesis via Suzuki Polycondensation

The first report, to the best of our knowledge, on continuous flow synthesis of polymers for organic electronics was mentioned in a patent filed by Merck GmbH [53]. They reported the synthesis of OLED material based on spirofluorene and arylamine via Suzuki

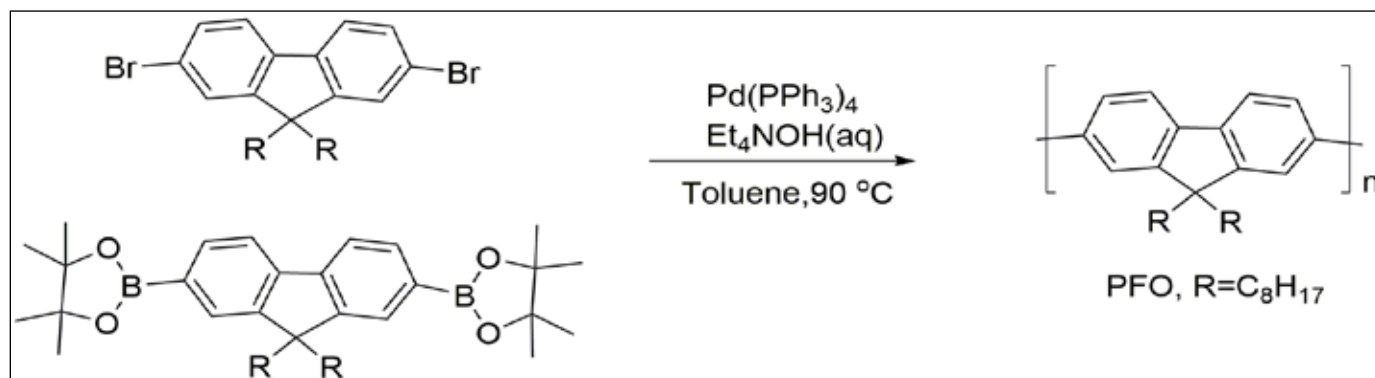
Polycondensation. Comparison of batch reaction and flow reaction showed a vivid reduction in the reaction time from 42 min to 9 min with a comparable molecular weight and less PDI of the polymer. Electroluminescence properties of the continuous flow synthesized polymers were better than the batch synthesized polymer. (Table 1) This shows the ability of the technology to reduce the reaction time and improve the profile of materials synthesized and opens up the scope for carrying out various reactions via continuous flow process.

**Table 1. Reaction conditions, molecular mass data and device data of Suzuki Polycondensation reaction of polymer P2 [53].**

Polymer P2	Reaction time(min)	Mw (kDa)	PDI	Electroluminescence properties		
				cd/A	U	Life
Flow	9	240	2.18	4.8	3.9	2000
Batch	42	460	3.07	3.6	4.2	900

First, open literature on continuous flow synthesis of conjugated polymers was reported by Seyler *et al.* via Suzuki Polycondensation [54]. They synthesized poly(9,9-dioctylfluorene) (PFO), (Scheme 1) and a carbazole-benzothiadiazole based polymer PCDHTBT [55] via continuous flow synthesis and compared with the batch results. They used a commercial flow reactor Vapourtec with a reactor volume of 10 mL for Suzuki Polycondensation of the polymers mentioned above.

Even though batch and flow gave similar molecular weights, there was a significant reduction in reaction time as compared to the batch reaction. (Table 2) This reduction in time is attributed to the elevated reaction temperature possible in continuous flow synthesis which is not possible in a batch reaction. So by exploring the novel process window, the reaction is performed at a higher temperature



Scheme 1: PFO synthesis via Suzuki polycondensation



**Table 2. Reaction conditions and molecular mass data of Suzuki, Stille and Gilch Reaction in batch and flow [54]**

Polymer	Method	Reaction time (h)	Temperature (°C)	Mw (kDa)	PDI	Yield(%)
PFO	Batch	2	90	71	3.4	64
PFO	Flow	1	90	39	3.4	70
PFO	Flow	1	120	63	2.8	90
PFO	Flow	0.5	120	62	3.1	70
PCDHTBT	Batch	14	90	25	1.6	74
PCDHTBT	Flow	2	120	23	1.9	79
PTB	Batch	14	130	28	1.9	89
PTB	Flow	1	170	29	1.7	75
MEH-PPV	Batch	5	25	121	1.7	82
MEH-PPV	Flow	0.5	25	90	1.6	72

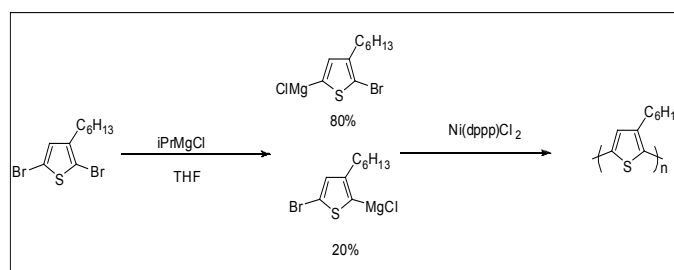
and lower residence time. In addition to the advantages of the flow process authors have also mentioned the difficulties of the processes. The solubility of the substrates in the solvent is very crucial for dosing of the reagents, and sometimes they modified the monomer molecules to aid the process [54]. Besides PFO and PCDHTBT, same researchers have performed Stille polycondensation of alternating thieno[3,4-b]thiophene and benzodithiophene polymer (PTB) and Gilch method for the synthesis of Poly[2-methoxy-5-(2-ethylhexyloxy)-1,4-phenylenevinylene (MEH-PPV) in batch and flow and compared the results of two processes (**Table 2**). Xylene was used as the solvent in the flow reaction of PTB at 170 °C, which is unattainable under normal batch reaction conditions and has aided the reaction to complete faster.

### 2.3 Continuous Flow Synthesis of regioregular-P3HT(rr-P3HT)

As mentioned earlier P3HT is one of the organic electronic materials widely used and available commercially in large scale, but the cost of buying large quantities is prohibitive. Though P3HT is produced in large quantities via batch synthesis reproducibility and properties are always a setback in research and development. There is a considerable effect of the properties like molecular weight, PDI, chemical defects, end groups and impurities on the electronic properties of the organic electronic devices. Besides the above-said problems, the fast polymerization kinetics in the P3HT synthesis affects the processing parameters such as heat exchange, and stirring become critical as the batch size increases, which can efficiently be taken care of by the continuous flow synthesis.

Among many synthetic pathways, P3HT is widely synthesized by Grignard Metathesis (GRIM) polymerization route established by Mc Cullough [56]. In GRIM

polymerization 2,5 dibromo derivative of 3-hexylthiophene is activated first with one equivalent of Grignard reagent (Isopropyl Grignard) in tetrahydrofuran (THF) which yields two regioisomers. The major isomer undergoes quasi-living chain-growth in the presence of the catalyst [1,3-bis(diphosphinopropane)]-nickel(II) chloride ( $\text{Ni}(\text{dppp})\text{Cl}_2$ ) to form regioregular P3HT and the minority isomer being sterically hindered do not take part in the reaction (**Scheme 2**). The mechanism of the polymerization reaction is chain growth and is classified as a pseudo-living process and is also named as Kumada Catalyst-Transfer Polymerisation (KCTP) and in this process catalyst, monomer ratio can be adjusted to get the desired molecular weight of the polymer.



**Scheme 2:** Synthesis of regioregular poly(3-hexylthiophene) by Grignard Metathesis (GRIM) polymerization.

Though GRIM polymerization is the widely accepted method for the synthesis of rr-P3HT, it has a few shortcomings like insolubility of catalyst in the solvent and thereby poor mixing of the ultrafast reaction and poor heat transfer in large batches leading to high PDI and low molecular weight. Also, each polymer chain has a chemical defect which affects the mobility of the organic electronic devices. Many groups had tried addressing the insolubility of the catalyst in different ways like making soluble catalyst and changing the solvent to dissolve

the catalyst to carry out the reaction. All these attempts make the synthesis of rr-P3HT flow amenable as well, and continuous flow synthesis of rr-P3HT can help in making of large quantities of the material without batch to batch variation.

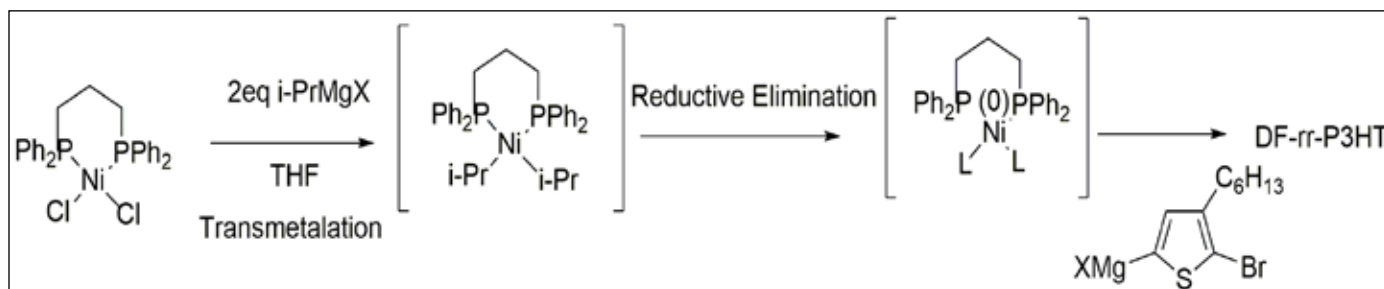
Research groups including ours have explored the rr-P3HT synthesis using continuous flow process and have used different reactors for carrying out the synthesis. GRIM polymerization is carried out under extreme dry condition, so the pumping mechanism, as well as the reactors, should be perfectly dry to carry out the reaction in the continuous flow process successfully. To circumvent the problem, a droplet-based micro-reactor system was used for the synthesis of P3HT by Bannock *et al.* [43,57]. In this method they used polytetrafluoro ethylene (PTFE) tubing with inner diameter 1mm as the reactor. Almost monodisperse droplets were created by injecting monomer solution into a stream of carrier liquid (perfluorinated polyether (PFPE)) which is immiscible and uniform dispersion of catalyst can be added with carrier liquid or can be added as a second droplet. P3HT produced using the droplet-based microreactor was used for making OPV devices and achieved similar power conversion efficiencies as obtained for batch synthesized P3HT, showing that continuous production using this method avoid batch to batch variation.

Further, the solubility of reagents and catalyst in the desired solvent is very crucial to carry out continuous flow synthesis, and insolubility of the GRIM catalyst (1,3-bis(diphenylphosphino)propane nickel(II) chloride) in polymerization solvent was a bottleneck. To circumvent this Kumar and co-workers used ethylene dioxythiophene (EDOT) as a solvent to dissolve the catalyst and successfully carried out continuous flow synthesis of P3HT [58]. A higher concentration of monomer (500 mM) was used in the continuous flow synthesis that helped in the large-scale synthesis with reduced chemical waste and the material had low PDI(1.2) and optoelectronic properties were better compared to batch synthesized P3HT.

Kumar and co-workers also synthesized defect-free rr-P3HT (**Scheme 3**) using 2-bromo-3-hexyl-5-iodothiophene and Ni(0) catalyst in THF and compared the batch and flow synthesis. Charge carrier mobility of the devices made from defect-free rr-P3HT was initially  $1.2 \text{ cm}^2/\text{V s}$  [59], and on using floating film transfer method for deposition, the mobility increased to  $6.3 \text{ cm}^2/\text{V s}$  [60] on an average ( $8 \text{ cm}^2/\text{V s}$  as highest). Using the defect-free rr-P3HT (DF-rr-P3HT) Kabra and co-workers studied the effect of regioregularity of P3HT on the charge transport properties and bimolecular recombination rates of polymer-based solar cells and found improvement in PCE which is due to defect-free nature of the material [61].

Because of the moderate solubility of Ni(dppp)Cl<sub>2</sub> in tetrahydrofuran (THF), Seyler *et al.* used tolyl-functionalized nickel complex instead of the conventional catalyst. Also, the ligand dissociation phenomenon of Ni(dppp)Cl<sub>2</sub> observed in THF was addressed by an alternative approach by dissolving the catalyst in 1,2-Dichlorobenzene. Batch reactions were initially carried out followed by the polymerization of 3-hexylthiophene in flow reactor yielding polymers of polydispersity index between 1.5 to 1.8 and the reaction time was also reduced to eighteen minutes [62]. Bench-top commercial flow reactors were used for the controlled synthesis of P3HT. Photovoltaic devices were made using P3HT synthesized via flow, batch and commercially available P3HT and all gave comparable power conversion efficiencies.

Bannock *et al.* performed droplet flow synthesis of P3HT using a green solvent 2-methyl tetrahydrofuran (2-MeTHF) [63]. The continuous flow process used soluble catalyst Ni(dppp)Br<sub>2</sub> instead of the conventional GRIM catalyst. The higher boiling point of the solvent enhanced the reaction rate, and in less than a minute a 44 kDa sample was obtained via continuous flow synthesis. All these work throw light into the use of continuous flow synthesis for the making organic electronics materials.



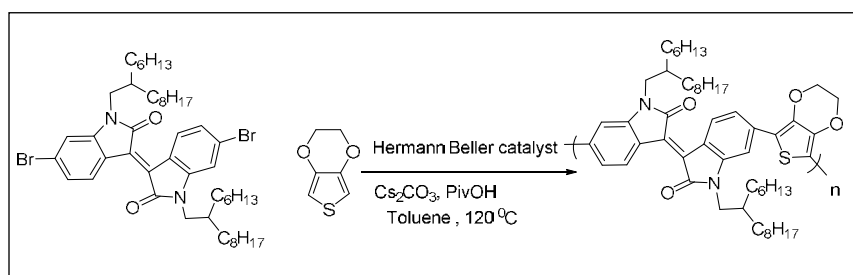
**Scheme 3:** Ni(0) catalyzed synthesis of DF-rr-P3HT

## 2.4 Continuous Flow Synthesis of Conjugated Polymers via C-H Arylation

C-H arylation polymerization is considered as a very efficient way of polymerization as it has less number of synthetic steps and avoids toxic intermediates. It seemed impossible to handle the reaction in continuous flow synthesis because handling a solid inorganic carbonate base was tricky in the standard fluidic set-up of continuous flow synthesis. But different reactor geometries are available to take care of such reactions and using a column reactor filled with the inorganic carbonate base the continuous flow reaction was successfully carried out by pumping the soluble substrate and catalyst [64]. A donor-acceptor polymer based on Isoindigo and EDOT was synthesized using direct hetero arylation polymerization via continuous flow synthesis (**Scheme 4**). The commercially available Vapourtec reactor was used in the continuous flow synthesis and compared the polymer properties, and device properties with the batch synthesized polymer. They found that the continuous flow process gave reproducible molecular weight ( $M_w = 108 \pm 10$  kg/mol) when three consecutive reactions were performed using two freshly prepared columns, but in batch, there was a huge variation of molecular weight.

Gobalasingham *et al.* also reported direct arylation polymerization and synthesized poly[(2,5-bis(2-hexyldecyloxy)phenylene)-*alt*-(4,7-di(thiophene-2-yl)-benzo[c][1,2,5]thiadiazole)] (PPDTBT). PPDTBT is considered as a roll-to-roll compatible conjugated polymer, and the scaled synthesis of the material via continuous flow synthesis enables the evaluation of the suitability of the process for many high-performance materials. PPDTBT is synthesized via Stille cross-coupling reaction, and the polymer synthesized via continuous flow direct arylation is compared by making a solar cell and achieved a PCE of 3.5% for 1 cm<sup>2</sup> device which is comparable to the polymer prepared via Stille route [65].

## 2.5 Continuous flow synthesis of Poly(Ethyl-Hexyl-3,4-Propylenedioxythiophene): Poly(ProDOT(CH<sub>2</sub>OEtHx)<sub>2</sub>)



Scheme 4: Synthesis of PiiEDOT via continuous flow process

Poly(oxythiophenes) are widely used in the organic electronics industry in electrochromic applications [66]. Widely used electrochromic polymers are based on ethylene dioxythiophene and propylenedioxy thiophene. Various substituents are introduced to fine-tune the final properties and improve the processing, and alkyl substitution is widely used for increasing solubility in organic solvents. Syntheses and characterization of the polymer of Ethyl-Hexyl-3,4-Propylenedioxythiophene were carried out in a single step oxidative polymerization by continuous flow synthesis by Shilpa *et al.* [67]. Ferric Chloride was used as the catalyst for the oxidative polymerization of ProDOT(CH<sub>2</sub>OEtHx)<sub>2</sub> dissolved in 1:1 ethyl acetate: toluene mixture. High molecular weight (1800 kDa) polymer was obtained in 9-minute resident time in the continuous flow process. This being a single step reaction with an inexpensive oxidant coupled with continuous flow synthesis can be used for the commercial synthesis of the polymer. Other polymers which are used in electrochromic devices can be chosen for synthesis via continuous flow process.

## 2.6 Continuous Flow Synthesis of Conjugated Polymers via Oxidative Polymerization

Polyaniline and polypyrrole are also very vital conjugated polymers as they are widely used Electromagnetic Interference (EMI) shielding [68], corrosion protection [69], Sensors [70,71], etc. Batch syntheses of these polymers are extensively carried out [72-74], but large scale and high throughput synthesis of conjugated polymer nanofibers are not yet reported. Bajpai *et al.* used continuous flow synthesis for synthesizing nanofibres of polyaniline and polypyrrole via oxidative polymerization [75]. Scanning Electron Microscopy image and Transmission Electron Microscopy image (Figure 1 and Figure 2) clearly shows the formation of nanofibres of the polymer.

The BET surface area of polymeric nanofibers synthesized via continuous flow process was found much higher (473 vs. 34 m<sup>2</sup>/g) than the nanofibers synthesized via batch process. The enhanced surface

area is beneficial in many applications like sensors, EMI shielding, corrosion resistance and electrochemical capacitors. The conventional batch methods for the bulk production of polyaniline nanofibers lands up in agglomerates due to secondary nucleation, and continuous flow synthesis avoids the secondary nucleation and produces nanofibers in high throughput as high as 20 g/hr.

## Conclusion and Future Outlook

Organic electronics is an area widely explored by multidisciplinary scientists and researchers, and the role of chemists in designing and synthesizing molecules for organic electronics are exemplary. Chemists are the people, who can really make use of the technology of continuous flow process, by keeping aside the traditional thinking and open-up the hands for the upcoming technology. The limited acceptance of the technology for conjugated polymer synthesis is because of lack of exposure of synthetic polymer chemists to flow process and the reluctance to shift from the classical batch techniques. When continuous

flow synthesis is compared with batch synthesis, the operation costs and labor required is usually less, coupled with increased safety and low footprint. Considering the enormous potential of continuous flow process, it can be a game changer in the preparation and purification of organic electronics materials. We made a humble effort to summarize the state-of-the-art developments in the area of conjugated polymers via continuous flow processing. However, there are still challenges like insoluble nature of monomers which makes dosing difficult and insolubility or limited solubility of the polymers which clogs the reactor. With the growth of the technology, finding the best reactor

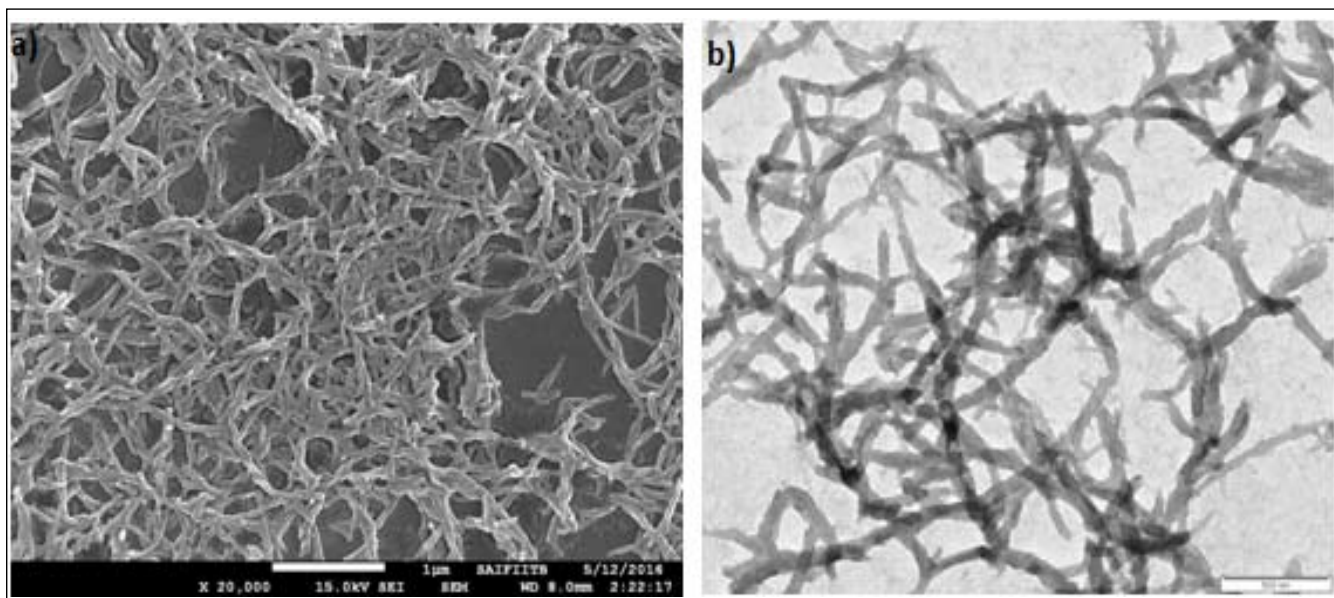


Fig. 1: Scanning Electron Microscopy image (a) and Transmission Electron Microscopy image (b) of Polyaniline synthesized by continuous flow process.

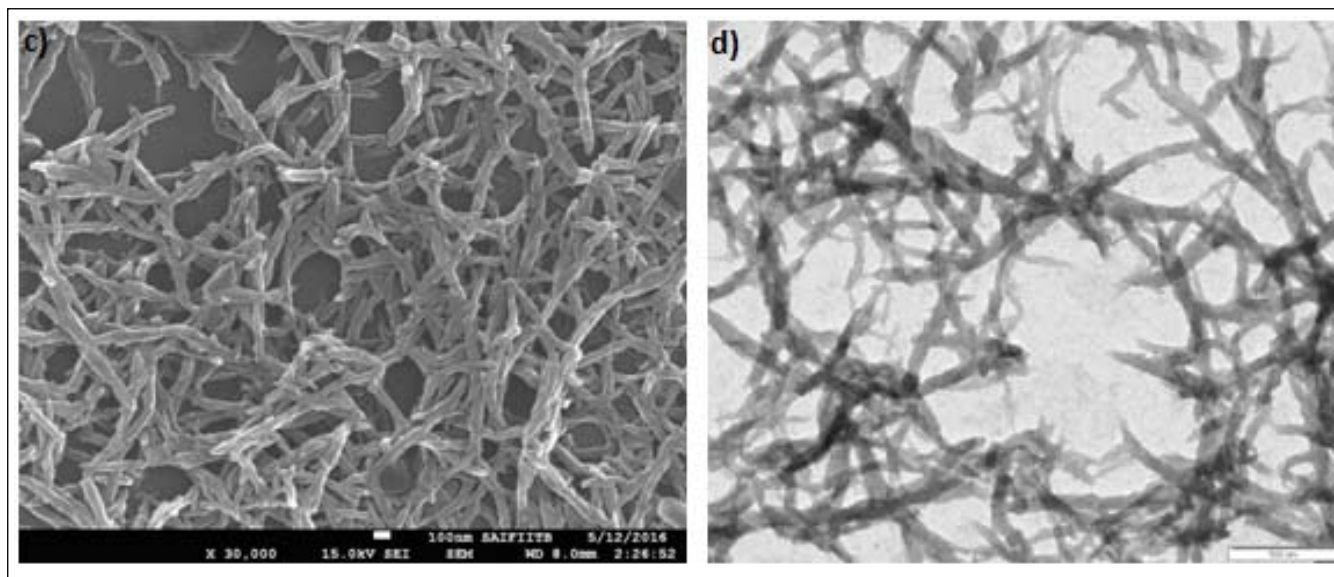


Fig. 2: Scanning Electron Microscopy image(c) and Transmission Electron Microscopy image (d) of Polypyrrole synthesized by continuous flow process.

geometry and efficient pumping mechanism can help us to move forward in this direction. Though the research in the area till date is less, the achievements obtained are worth mentioning which holds a great promise for the synthesis of organic electronic materials.

## References

1. S. R. Forrest, *Nature*, 2004, 428, 911.
2. Editorial, *Nature Nanotechnology*, 2009, 4, 607.
3. Y. Lei; P. Deng; J. Li; M. Lin; F. Zhu; T.-W. Ng; C.-S. Lee; B. S. Ong, *Scientific Reports*, 2016, 6, 24476.
4. F. C. Krebs; J. Alstrup; H. Spanggaard; K. Larsen; E. Kold, *Solar Energy Materials and Solar Cells*, 2004, 83, 293.
5. F. C. Krebs, *Organic Electronics*, 2009, 10, 761.
6. O. Ostroverkhova; Editor *Handbook of Organic Materials for Optical and (Opto) Electronic Devices: Properties and Applications*. [In: Woodhead Publ. Ser. Electron. Opt. Mater., 2013; 39]; Woodhead Publishing Ltd., 2013.
7. R. Das and P. Harrop Printed, Organic & Flexible Electronics Forecasts, Players & Opportunities 2013-2023. [Online Early Access]. Published Online: 2013.
8. W. Zhao; S. Li; H. Yao; S. Zhang; Y. Zhang; B. Yang; J. Hou, *Journal of the American Chemical Society*, 2017, 139, 7148.
9. C. Reese; M. Roberts; M.-m. Ling; Z. Bao, *Materials Today*, 2004, 7, 20.
10. I. McCulloch, *Advanced Materials*, 2013, 25, 1811.
11. J. Mei; Y. Diao; A. L. Appleton; L. Fang; Z. Bao, *Journal of the American Chemical Society*, 2013, 135, 6724.
12. M. Urien; G. Wantz; E. Cloutet; L. Hirsch; P. Tardy; L. Vignau; H. Cramail; J.-P. Parneix, *Organic Electronics*, 2007, 8, 727.
13. F. C. Krebs; N. Espinosa; M. Hösel; R. R. Søndergaard; M. Jørgensen, *Advanced Materials*, 2014, 26, 29.
14. G. Mueller; T. Gaupp; F. Wahl; G. Wille, *Chimia*, 2006, 60, 618.
15. H. Seyler; S. Haid; T.-H. Kwon; D. J. Jones; P. Baeuerle; A. B. Holmes; W. W. H. Wong, *Aust. J. Chem.*, 2013, 66, 151.
16. M. B. Plutschack; B. Pieber; K. Gilmore; P. H. Seeberger, *Chemical Reviews*, 2017, 117, 11796.
17. H. R. Sahoo; J. G. Kralj; K. F. Jensen, *Angewandte Chemie*, 2007, 119, 5806.
18. A. R. Bogdan; S. L. Poe; D. C. Kubis; S. J. Broadwater; D. T. McQuade, *Angew. Chem., Int. Ed.*, 2009, 48, 8547.
19. J. C. Pastre; D. L. Browne; S. V. Ley, *Chem. Soc. Rev.*, 2013, 42, 8849.
20. K. Booker-Milburn, *Nat Chem*, 2012, 4, 433.
21. V. Hessel; D. Kralisch; N. Kockmann; T. Noël; Q. Wang, *ChemSusChem*, 2013, 6, 746.
22. L. Malet-Sanz; F. Susanne, *Journal of Medicinal Chemistry*, 2012, 55, 4062.
23. R. M. Myers; D. E. Fitzpatrick; R. M. Turner; S. V. Ley, *Chem. - Eur. J.*, 2014, 20, 12348.
24. R. L. Hartman; J. P. McMullen; K. F. Jensen, *Angew. Chem., Int. Ed.*, 2011, 50, 7502.
25. K. F. Jensen, *AIChE J.*, 2017, 63, 858.
26. S. V. Ley, *The Chemical Record*, 2012, 12, 378.
27. J. Wegner; S. Ceylan; A. Kirschning, *Advanced Synthesis & Catalysis*, 2012, 354, 17.
28. S. V. Ley; D. E. Fitzpatrick; R. M. Myers; C. Battilocchio; R. J. Ingham, *Angew. Chem., Int. Ed.*, 2015, 54, 10122.
29. C. Wiles; P. Watts, *Chem. Comm.*, 2011, 47, 6512.
30. C. Wiles; P. Watts, *Green Chemistry*, 2014, 16, 55.
31. B. Gutmann; D. Cantillo; C. O. Kappe, *Angew. Chem., Int. Ed.*, 2015, 54, 6688.
32. G. Jas; A. Kirschning, *Chemistry – A European Journal*, 2003, 9, 5708.
33. J. A. M. Lummiss; P. D. Morse; R. L. Beingessner; T. F. Jamison, *The Chemical Record*, 2017, 17, 667.
34. B. P. Mason; K. E. Price; J. L. Steinbacher; A. R. Bogdan; D. T. McQuade, *Chemical Reviews*, 2007, 107, 2300.
35. A. J. Mijalis; D. A. Thomas Iii; M. D. Simon; A. Adamo; R. Beaumont; K. F. Jensen; B. L. Pentelute, *Nat Chem Biol*, 2017, advance online publication.
36. A. Mehta. The flow revolution, <https://www.chemistryworld.com/feature/the-flow-revolution/2500496.article>. [Online Early Access]. Published Online: 2017. (accessed 26/4/2017).
37. C. Allemann; R. Marti; O. Vorlet; O. Martin; P. Riedlberger; T. Leonhardt; A. Gössi; W. Riedl; J.-M. Segura; M. Zinn; S. Crelier, *CHIMIA International Journal for Chemistry*, 2017, 71, 525.
38. B.-A. Daniel; R. F. P. J. T., *Journal of Flow Chemistry*, 2017, 7, 157.
39. J. P. McMullen; K. F. Jensen, *Annu. Rev. Anal. Chem.*, 2010, 3, 19.
40. B. J. Reizman; Y.-M. Wang; S. L. Buchwald; K. F. Jensen, *Reaction Chemistry & Engineering*, 2016, 1, 658.
41. Y. Kikutani; M. Ueno; H. Hisamoto; M. Tokeshi; T. Kitamori, *QSAR & Combinatorial Science*, 2005, 24, 742.
42. V. Sans; L. Cronin, *Chem. Soc. Rev.*, 2016, 45, 2032.
43. J. H. Bannock; S. H. Krishnadasan; M. Heeney; J. C. de Mello, *Materials Horizons*, 2014, 1, 373.
44. M. Helgesen; J. E. Carle; G. A. dos Reis Benatto; R. R. Søndergaard; M. Jørgensen; E. Bundgaard; F. C. Krebs, *Adv. Energy Mater.*, 2015, 5, 1401996/1.
45. G. Denzler; M. C. Scharber; C. J. Brabec, *Advanced Materials*, 2009, 21, 1323.
46. R. Po; M. Maggini; N. Camaioni, *The Journal of Physical Chemistry C*, 2010, 114, 695.
47. B. C. Thompson; J. M. J. Frechet, *Angew Chem Int Ed Engl*, 2008, 47, 58.
48. S. Guenes; H. Neugebauer; N. S. Sariciftci, *Chem. Rev. (Washington, DC, U. S.)*, 2007, 107, 1324.
49. X. Gu; Y. Zhou; K. Gu; T. Kurosawa; Y. Guo; Y. Li; H. Lin; B. C. Schroeder; H. Yan; F. Molina-Lopez; C. J. Tassone; C. Wang; S. C. B. Mannsfeld; H. Yan; D. Zhao; M. F. Toney; Z. Bao, *Advanced Energy Materials*, 2017, 7, 1602742.
50. J. J. Rubio Arias; M. d. F. Vieira Marques, *Reactive and Functional Polymers*, 2017, 113, 58.
51. S. Ludwigs *P3HT Revisited – from Molecular Scale to Solar Cell Devices*; Springer, 2014.

52. J. H. Bannock; N. D. Treat; M. Chabiny; N. Stingelin; M. Heeney; J. C. de Mello, *Scientific Reports*.**2016**, 6, 23651.
53. N. Schulte; E. Breuning; H. Spreitzer; Merck Patent GmbH, US 2008/0207851 A1: 2008.
54. H. Seyler; D. J. Jones; A. B. Holmes; W. W. H. Wong, *Chem. Commun. (Cambridge, U. K.)*.**2012**, 48, 1598.
55. J. Kim; Y. S. Kwon; W. S. Shin; S.-J. Moon; T. Park, *Macromolecules*.**2011**, 44, 1909.
56. R. S. Loewe; S. M. Khersonsky; R. D. McCullough, *Adv. Mater. (Weinheim, Ger.)*.**1999**, 11, 250.
57. J. H. Bannock; S. H. Krishnadasan; A. M. Nightingale; C. P. Yau; K. Khaw; D. Burkitt; J. J. M. Halls; M. Heeney; J. C. de Mello, *Advanced Functional Materials*, **2013**, 23, 2123.
58. A. Kumar; J. Hasan; A. Majji; A. Avhale; S. Gopinathan; P. Sharma; D. Tarange; R. Bajpai; A. Kumar, *Journal of Flow Chemistry*, **2014**, 4, 206.
59. A. Nawaz; M. S. Meruvia; D. L. Tarange; S. P. Gopinathan; A. Kumar; A. Kumar; H. Bhunia; A. J. Pal; I. A. Hümmelgen, *Organic Electronics*, **2016**, 38, 89.
60. A. Nawaz; A. Kumar; I. A. Hümmelgen, *Organic Electronics*.**2017**, 51, 94.
61. C. Naresh; C. Y. L. Amelia; K. Anil; R. M. Christopher; K. Dinesh, *Journal of Physics D: Applied Physics*, **2018**, 51, 015501.
62. H. Seyler; J. Subbiah; D. J. Jones; A. B. Holmes; W. W. H. Wong, *Beilstein J. Org. Chem.*,**2013**, 9, 1492.
63. J. H. Bannock; W. Xu; T. Baïssas; M. Heeney; J. C. de Mello, *European Polymer Journal*.**2016**, 80, 240.
64. F. Grenier; B. R. Aich; Y.-Y. Lai; M. Guerette; A. B. Holmes; Y. Tao; W. W. H. Wong; M. Leclerc, *Chem. Mater.*, **2015**, 27, 2137.
65. N. S. Gobalasingham; B. C. Thompson; J. E. Carle; F. C. Krebs; E. Bundgaard; M. Helgesen, *Macromol Rapid Commun*.**2017**, 38.
66. A. Kumar; S. P. Gopinathan; R. Singh In *Conjugated Polymers: A Practical Guide to Synthesis*; The Royal Society of Chemistry: 2014, p 201.
67. S. Ramesh. Optimization of polymerization of ProDOT (CH<sub>2</sub>OEtHx)<sub>2</sub> by batch process and continuous flow process, M. Sc Thesis, 2017, p 28.
68. S. K. Dhawan; N. Singh; D. Rodrigues, *Sci. Technol. Adv. Mater.*, **2003**, 4, 105.
69. B. Wessling, *Materials and Corrosion*.**1996**, 47, 439.
70. J. Huang; S. Virji; B. H. Weiller; R. B. Kaner, *Chem. - Eur. J.*,**2004**, 10, 1314.
71. B. H. Weiller; S. Virji; R. B. Kaner In 232nd ACS National Meeting, San Francisco, CA, United States, Sept. 10-14; American Chemical Society: 2006.
72. J. Huang; S. Virji; B. H. Weiller; R. B. Kaner, *Journal of the American Chemical Society*.**2003**, 125, 314.
73. X. Zhang; W. J. Goux; S. K. Manohar, *Journal of the American Chemical Society*.**2004**, 126, 4502.
74. P. Anilkumar; M. Jayakannan, *Journal of Applied Polymer Science*.**2009**, 114, 3531.
75. R. Bajpai; A. Kumar India, Indian institute of Bombay, Indian Patent Application No 3030/MUM/2015, filed on 10 August 2015.



**Anil Kumar** is currently a Chair Professor at IIT Bombay, in the Department of Chemistry, Center for excellence in Nanoelectronics, National Center for Photovoltaic Research and Education and National Center for Excellence in Technologies for Internal Security. His group's research interest are in the area of continuous flow processes and printable optoelectronic devices based on conjugated polymers. In this direction, the main focus is on the development of handheld explosive sensors, electrochromic devices, thin film optoelectronic devices and transparent conductor etc. They have developed a state of the art continuous flow process lab and also conduct regular training programs and workshops in Continuous Flow Process to train the next generation of human resources in this important emerging technology. Based on the processes, he started a company "Sycon Polymers India Pvt Ltd" (<http://sycon.in/Home>) and another start-up is in pipeline. His group also has developed many technologies including transfer of technology in the domain of handheld explosive sensors and continuous flow processes. For his contribution in this field, he has been awarded with the 2017 NASI-RIL Platinum Jubilee National Award for application-oriented innovations.

Apart from research, his other hobbies are teaching, sports, technical financial analysis, magic and music. He has developed an outreach program based on "Science & Magic" to promote teaching and practice of science among students and research scholars of different grades and has been conducting such workshops around the country.



**Sreelekha P Gopinathan** graduated from Centre for Research in Nanotechnology and Science (CRNTS), IIT Bombay under the guidance of Prof Anil Kumar in October 2017. She worked in the area of flow chemistry and her PhD dissertation is titled "Continuous Flow Synthesis- Process Intensification of Bromination and Transesterification". She did her B Tech and M Tech from the Department of Polymer Science and Rubber Technology, Cochin University of Science and Technology, Kerala. Presently she is working as a Senior Project Technical Assistant in CRNTS, IIT Bombay.







**SOCIETY FOR MATERIALS CHEMISTRY (SMC)**  
(Reg. No. - Maharashtra, Mumbai/1229/2008/GBBSD)  
c/o Chemistry Division  
Bhabha Atomic Research Centre, Mumbai 400 085

**APPLICATION FOR MEMBERSHIP**

Please enroll me as a Life member of the *Society for Materials Chemistry (SMC)*. My particulars are as follows:

Name : \_\_\_\_\_

Educational Qualifications : \_\_\_\_\_

Field of Specialization : \_\_\_\_\_  
\_\_\_\_\_

Official Address : \_\_\_\_\_  
\_\_\_\_\_

Telephone No. (Off.) : \_\_\_\_\_

Residential Address : \_\_\_\_\_  
\_\_\_\_\_

Telephone No. (Res.) : \_\_\_\_\_

Address for Correspondence : Home/Office (Please tick one of the options)

E-mail Address : \_\_\_\_\_

Subscription Details

Mode of Payment : Cheque/DD/Cash  
(Cheque/DD should be drawn in favor of "*Society for Materials Chemistry*" for Rs. 1000/- payable at Mumbai. For out-station *non-multi-city* cheques, please include Rs.50/- as additional charge for bank clearance.

Number :

Dated :

Drawn on Bank & Branch :

Amount :

Place:

Date:

Signature

Registration Number: \_\_\_\_\_ (To be allotted by SMC office)



*Printed by:*

**Ebenezer Printing House**

Unit No. 5 & 11, 2nd Floor, Hind Service Industries

Veer Savarkar Marg, Shivaji Park Sea-Face, Dadar (W), Mumbai - 400 028

Tel.: 2446 2632 / 2446 3872 Tel Fax: 2444 9765 E-mail: [outworkeph@gmail.com](mailto:outworkeph@gmail.com)

## In this issue

	Feature Articles	Page No.
1.	<b>Alkaline Pyramidal Texturing Processes for Industrial Monocrystalline Silicon Wafer Solar Cells</b> <i>Prabir Kanti Basu</i>	1
2.	<b>Role of Colloids and Solvent Chemistry in Metal Halide Perovskites Thin Film and Crystal Formation.</b> <i>Pabitra K. Nayak</i>	7
3.	<b>Controlling Nucleation and Growth to Engineer Nanocrystal Composition and Morphology</b> <i>Rekha Mahadevu, Dev Kumar Thapa, Biswajit Bhattacharyya and Anshu Pandey</i>	13
4.	<b>Advances in Flexible Thin-Film Transistors and Their Applications</b> <i>Ashutosh Kumar Tripathi, Ishan Choudhary, Deepak</i>	21
5.	<b>Conjugated Polymers: New Insights via Continuous Flow Syntheses</b> <i>Anil Kumar and Sreelekha P Gopinathan</i>	28

Published by  
**Society for Materials Chemistry**  
C/o. Chemistry Division  
Bhabha Atomic Research Centre, Trombay, Mumbai 40085  
e-mail: socmatchem@gmail.com, Tel: 91-22-25592001